Thermokarst lake dynamics in the continuous and isolated permafrost zones, Mongolia

DOCTORAL THESIS

BY

ADIYA SARUULZAYA

Division of Earth System Science
Graduate School of Environmental Science
Hokkaido University

Sapporo, Japan

February 2017

Abstract

Thermokarst lakes are one of the most common features on the moist depressions and valleys in Mongolian permafrost region. Although, the spatiotemporal changes of thermokarst lake dynamics have not been investigated in the region so far. Thermokarst lakes are defined as lakes that occupy generally closed depressions formed by the settlement of ground following of ice rich permafrost or melting of massive ice. After a thermokarst lake has formed, the lake size may change due to continued permafrost thaw, variations in air temperature, potential evapotranspiration and precipitation. The factors controlling their dynamics in decadal scale have been controversial and still the main research topics of permafrost regions. The aims of this study are (1) to provide quantitative information on the spatiotemporal changes of thermokarst lakes in Mongolia, (2) to categorize the extracted lake areas into four distinct size categories, (3) to calculate volume changes of thermokarst lakes, and (4) to address the effects of the long-term trends of hydro-climatic regimes and permafrost degradation on the changes of lakes.

This study used the high spatial resolution Corona KH-4, KH-4A and KH-4B (1962-1968), Landsat ETM+ (1999-2001), and ALOS/AVNIR-2 (2006-2007) satellite images to investigate changes of thermokarst lake dynamics at seven different study sites in the continuous and isolated permafrost zones of Mongolia. Lakes larger than 0.1 ha (1000 m^2) were analyzed using remote sensing and geographical information system tools. On the other hand, this study used the NCEP/NCAR data for air temperature, and APHRODITE data for precipitation.

Between 1962 and 2007, the total number and area of lakes increased by +21% (347 to 420) and +7% (3680 ha to 3936 ha) in the continuous permafrost zone, respectively. These changes

correspond to the appearance of 85 new lakes (166 ha) during the last 45 years. In contrast, lakes in the isolated permafrost zone have decreased by −42% (118 to 68) in number and −12% (422 ha to 371 ha) in area from 1962 to 2007. The changes in lake area and number are likely attributed to shifts in climate regimes and local permafrost conditions. In order, the dramatic increase in number of smaller lakes with sizes between 0.1-1 ha and 1-10 ha compared to larger lakes (10-100 ha and 100-1000 ha) in the continuous permafrost zone is likely as a result of permafrost degradation due to increasing temperature and evaporations. However, small lakes (0.1 - 1 ha) had a significant reduction in number in the isolated permafrost zone. On the other hand, the volume changes of thermokarst lakes are increased in the continuous permafrost zone, which is likely attributed to the increasing area and number of lakes in the depression. In the isolated permafrost zone, in contrast, that the volume changes observed only negative values.

Since 1962, the mean annual air temperature and potential evapotranspiration are increased significantly in the northern continuous permafrost zone compared to the southern isolated permafrost zone. Due to ongoing atmospheric warming without any significant trend in annual precipitation, ice-rich permafrost has thawed, and the number and area of thermokarst lakes have accordingly developed in the continuous permafrost zone. Shrinking of thermokarst lakes in the isolated permafrost zone may be due to disappearing permafrost, deepening of the active layer, and increased water loss through surface evaporation and subsurface drainage.

This study provides the first baseline information of thermokarst lake changes across Mongolia, filling the gap in sub-Arctic lake inventories at regional scales such as the southern fringe of Siberian permafrost region.

Acknowledgements

First of all, I would like to express my most sincere appreciation to my supervisor, Associate Professor, Dr. Mamoru Ishikawa, Faculty of Environmental Science, Hokkaido University, for his constant supervision and support in every possible way to complete the thesis. Thanks for your high level requirements in scientific working and for supporting my participation in regional and international conferences. I will always be indebted to him for training me to embark on this scientific field.

I am greatly indebted to Dr. Yamkhin Jambaljav, Department of Permafrost, Institute of Geography and Geoecology, Mongolian Academy of Sciences, who gave me many constructive suggestions in field and office, and actively encouraged me through the course. I wish to express my enormous gratitude to Professor, Academician, and D.Sc. Dechingungaa Dorjgotov, former director of the Institute of Geography, Mongolian Academy of Sciences, for his partial financial support in this study.

I would like to express my enormous gratitude to Professor Dr. Takanobu Sawagaki, Faculty of Environmental Science, Hokkaido University, for his constructive suggestions, instructions, and comments during my initial stages of this study. I wish to express my cordial thanks to Associate Professor Dr. Tomonori Sato, Faculty of Environmental Science, Hokkaido University, for his comments and suggestions to improve this thesis. I must express my gratitude to Dr. Lamsal Damodar of Hokkaido University, for his help in processing of high-resolution images to orthorectify with the LPS.

I would like to appreciate all the members of the Course in Geoecology & Field Informatics, Graduate School of Environmental Science, Hokkaido University, for their assistance in various steps and also for their active participation in seminar and discussion.

I am deeply grateful to my parents, family, relatives, friends and well-wishers for their cooperation, patience, encouragement and concern for my research and study. They are the source of inspiration to complete my PhD thesis.

I would like to dedicate this work to my father D. Adiya and mother Sh. Altantsetseg, for teaching me the value of education, whose love and character will forever positively impact my life.

I am much thankful to my husband D. Otgonbaatar, our beautiful daughter O. Dulguun, son O. Naranbaatar, and my young brother A. Erdenedalai. They allowed me to concentrate on completing this dissertation and supported mentally during the course of this work. Without their help and encouragement, this study would not have been completed.

Finally, I would like to express my sincere appreciation to the Global Centre of Excellence (GCOE) program of Hokkaido University for supporting this study.

Contents

List of figures

List of photographic

No

List of tables

List of Abbreviations

ALOS	Advanced Land Observing Satellite
AVNIR-2	Advanced Visible and Near Infrared Radiometer type 2
A.S.L	Above Sea Level
APHRODITE	Asian Precipitation Highly Resolved Observational Data Integration towards Evaluation
ASTER	Advanced Spaceborne Thermal Emission and Reflection Radiometer
GDEM	Global Digital Elevation Model
GrADS	Grid Analysis Display System
GIS	Geography Information System
GPS	Global Positioning System
GCPs	Ground Control Points
ETM+	Enhanced Thematic Mapper Plus
JAXA	Japan Aerospace Exploration Agency
KH-4	Keyhole-4
KH-4A	Keyhole-4A
KH-4B	Keyhole-4B
LPS	Leica Photogrammetric Suite
MAAT	Mean annual air temperature
MSS	Multi-spectral Scanner
NASA	National Aeronautics and Space Administration
N/A	Not Available
NCEP	National Center for Environmental Prediction
NCAR	National Center for Atmospheric Research
PALSAR	Phased Array type L-band Synthetic Aperture Radar
P	Precipitation
PET	Potential Evapotranspiration
p	significance level
RMSE	Root Mean Square Error
TM	Thematic Mapper

r^2	coefficient of determination
WGS	World Geodetic System
UTM	Universal Transverse Mercator
Δ	Changes
$\Delta \mathbf{V_{1,2}}$	Volume changes of the lake
$\Delta \mathbf{H_{1,2}}$	Difference in depth between two successive depth contours
$h_{1,2,3}$	Lake level in different time periods as
$S_{1,2,3}$	Surface area of lake at depth

Chapter I. Introduction

1.1. Scientific background

Approximately 24% of the northern land surface is located in permafrost zones (Brown *et al*., 1997). Permafrost, defined as the ground that remains at or below 0°C for more than two years, can be differentiated by its spatial extent into continuous (90–100%), discontinuous (50–90%), sporadic (10–50%), and isolated (0–10%) zones (Figure 1.1), as well as by its thickness, the amount of ground ice present, and its temperature (van Everdingen, 1998). Recent global climate warming is occurring in the northern hemisphere at a much faster rate than in other parts of the world and therefore significantly affects permafrost regions, which has resulted in widespread permafrost degradation and also its disappearance in some regions (IPCC, 2013).

A typical form of that permafrost degradation involves the formation and growth of thermokarst lakes (Soloviev, 1962). Thermokarst lakes are defined as lakes that occupy generally closed depressions formed by the settlement of ground following of ice-rich permafrost or melting of massive ice (van Everdingen, 1998). Such lakes have mainly formed during the transition from late Pleistocene to Holocene and are a sign of local permafrost degradation following climate warming (Rampton, 1988; Walter *et al*., 2007). A thick overburden of unconsolidated sediments, and high ground ice content (above 30% by volume), this often results in the formation of thermokatst lakes in areas with lowland (Jones *et al*., 2011; Grosse *et al*., 2013). However, thermokarst lakes can also occur in perennially frozen peat lands, poorly consolidated and ice-rich bedrock, and in alpine permafrost, such as mountain valleys and plateaus (Sannel and Brown, 2010).

Thermokarst lakes are one of the most dynamic and widespread features in permafrost regions, covering up to 50% of the total land area of the northern hemisphere (Frohn *et al*., 2005; Hikel *et al*., 2007). Scientific interest in the interactions between thermokarst lakes, permafrost, and climate has increased over the last decades. Their importance to global climate change and northern high latitude landscape and permafrost-stored carbon cycling has been identified (Zimov *et al*., 1997; Walter *et al*., 2007). Therefore quantifying changes in thermokarst lake dynamics is of importance for understanding potential positive feedback to climate warming.

Historical observations of changes in thermokarst lake dynamics in permafrost regions have shown different trends over the last five to six decades using remote sensing imagery (Figure 1.1). Several studies from areas of discontinuous to isolated permafrost zones agree in general reduction in area and number of thermokarst lakes (Yoshikawa and Hinzman, 2003; Smith *et al*., 2005; Riordan *et al*., 2006; Andresen and Lougheed, 2014) attributed to evapotranspiration and permafrost degradation, resulting in lateral and subsurface drainage (Anderson *et al*., 2013). However, other studies in the continuous permafrost zone are more ambiguous with diverse responses to the effects of climate and permafrost including the area and number of thermokarst lakes increases (Smith *et al*., 2005; Jones *et al*., 2011; Luo *et al*., 2015), both increases and decreased (Plug *et al*., 2008; Labrecque *et al*., 2009), small changes (Hinkel *et al*., 2007). This ambiguity can be attributed primarily to regional differences in climate (air temperature, evapotranspiration, water balance) and permafrost conditions (ground ice content and active layer thickness). Consequently, the factors controlling their dynamics in decadal scale have been controversial and still the main research topics of permafrost regions.

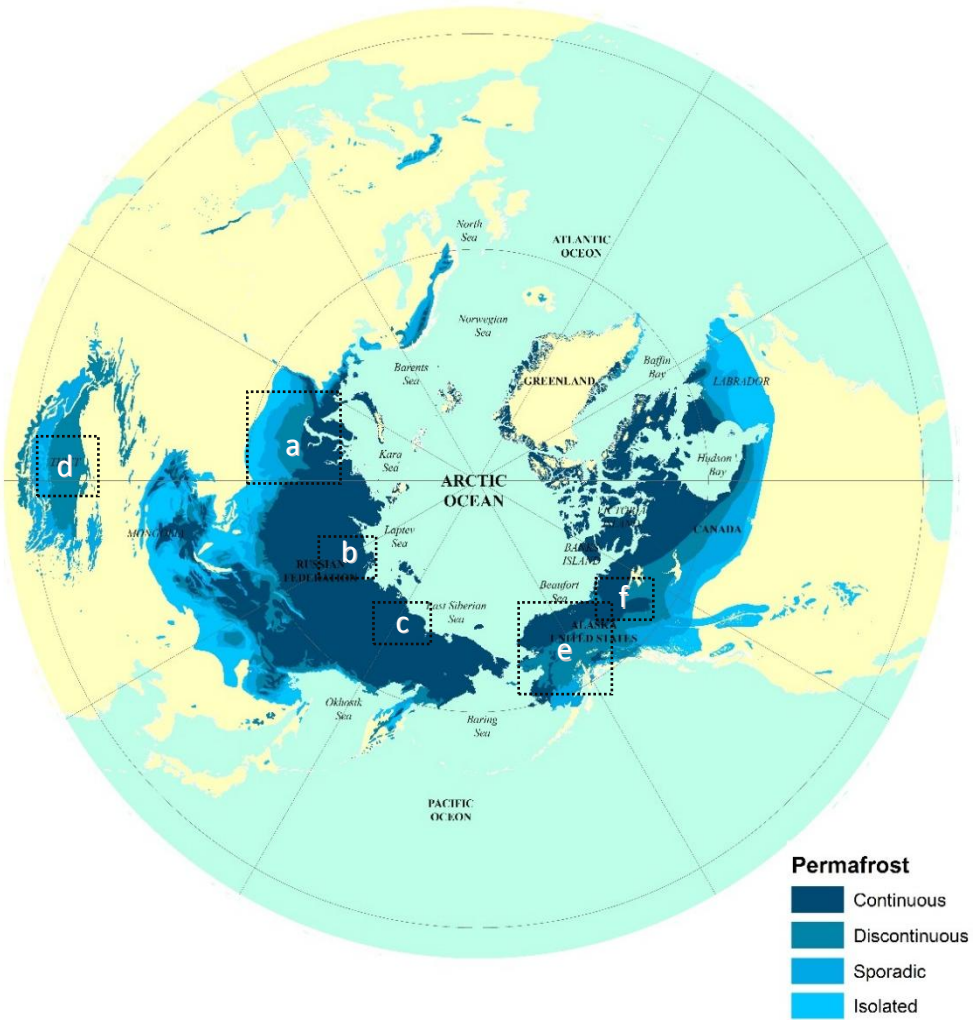

Figure 1.1. Permafrost distribution in the northern hemisphere (Brown *et al*., 1997). Map produced with data source (shape file) from Guido Grosse, University of Alaska Fairbanks. The dashed black rectangle represents the location of thermokarst lake change detection studies: a) Smith *et al*., 2005; Biskaborn *et al*., 2013; Karlsson *et al*., 2014; Manasypov *et al*., 2014, b) Morgenstern *et al*., 2011, c) Walter *et al*., 2006, d) Luo *et al*., 2015, Niu *et al*., 2011, e) Yoshikawa and Hinzman, 2003; Riordan *et al*., 2006; Hinkel *et al*., 2007, 2012; Jones *et al*., 2011; and Andresen and Lougheed, 2014, and f) Plug *et al*., 2008; Marsh *et al*., 2009; Labreque *et al*., 2009; Sannel and Brown, 2010.

1.2. Permafrost and thermokarst lakes in Mongolia

Mongolia is located in the southern fringe of Siberian permafrost (Figure 1.2). Permafrost, distribution changes according to geomorphologic and microclimatic conditions, exists in almost two thirds of Mongolia, predominantly distributed in the Altai, Hangai, Hovsgol, and Hentii mountain ranges and their surrounding areas (Jambaljav *et al*., 2013). The territory is characterized by mountain and arid-land permafrost. The permafrost divides into four altitudinal zones of permafrost distribution such as continuous, discontinuous, sporadic, and isolated (Figure 1.2-a). Permafrost of the country has temperatures close to zero degree and is expected to thaw drastically due to climate warming (Ishikawa *et al*., 2012). The average thickness and mean annual temperature in the areas of permafrost are 50 -100 m and −1 to −2˚C in river valleys and depressions, and 100 - 250 m and −1 to −3°C on mountains (Jambaljav *et al*., 2013). The thickness of the active layer in the continuous permafrost zone is 1 - 3 m, while it ranges 4 - 7 m in the discontinuous and isolated permafrost zone (Sharkhuu, 2011). Ground ice in this region is characterized mainly by low and moderate ice content in unconsolidated sediments (Figure 1.2-b). As shown the map, however, ice-rich permafrost (ice-patches) consists in the valleys and depressions under lacustrine and alluvial sediments. Continuous and ice-rich permafrost occurs in the northern areas of Mongolia with volumetric ice contents higher than 20% (Photo 1.1), while discontinuous, sporadic and isolated permafrost has low ice content in the southern areas (Brown *et al*., 1997). According to this environmental gradient would be interesting for comprehensive analysis of the factors controlling changes of thermokarst lake dynamics. Consequently, this study is focused on permafrost region of Mongolia.

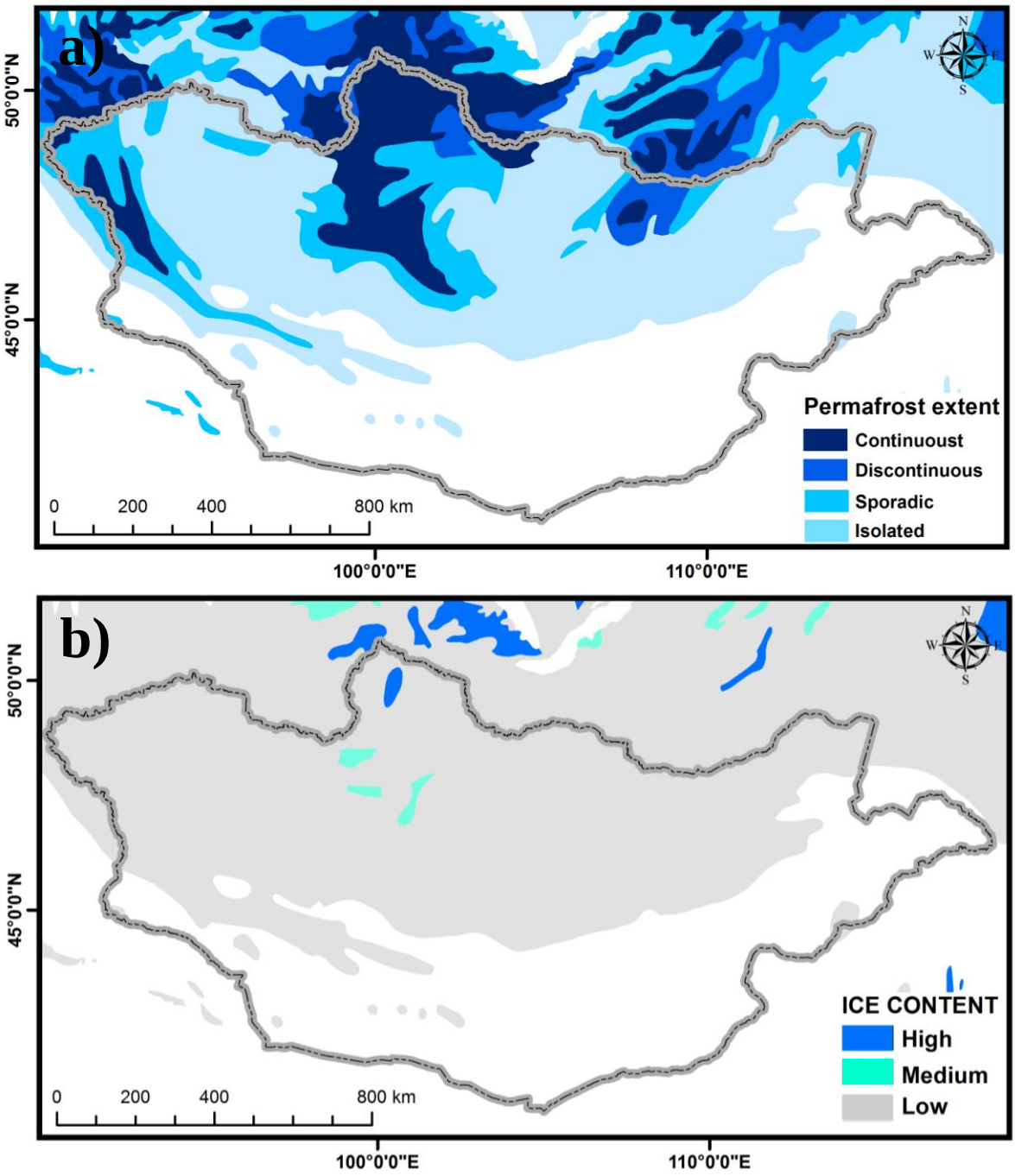

Figure 1.2. a) Permafrost distribution in Mongolia at the southern fringe of Siberian permafrost region. b) Distribution of ice content in the region (high > 20%, medium 10 – 20%, and low 0 – 10%).

Numerous thermokarst lakes exist on moist depression and river valleys within the four mountain ranges in Mongolia, where permafrost shows significant spatial variations in the extent and different ice contents. Information about thermokarst lakes in this region, at the southern fringe of Siberian permafrost, however, is remarkably scarce. Tserensodnom (2000) published a book entitled name “Lake catalog of Mongolia” which was indicated all lakes characteristics, morphology, and type (e.g., glacial, flood plain, thermokarst, and others) by each provinces across Mongolia. Other few researchers reported only the distribution of thermokarst lakes in some specific areas (Tumurbaatar, 2001; Nishida and Jamsran, 2009; Sharkhuu, 2011). However, these studies did not show the long-term changes of thermokarst lakes dynamics, the spatiotemporal changes of these lakes have not been investigated in Mongolia so far.

Photo 1.1. Exposure of ice-rich deposits at the Darkhad depression, in the northern continuous permafrost zone, Mongolia. Photo was taken by researchers of Permafrost Department at the Institute of Geography and Geoecology, Mongolian Academy of Sciences.

1.3. Research objectives

In light of the above background, this study aims i) to provide quantitative information on the temporal and spatial changes of thermokarst lakes at seven sites in the continuous and isolated permafrost zones of Mongolia, ii) to categorize the extracted lake areas into four distinct classes in order to better understand the lake dynamics of individual lake size categories, iii) to calculate volume changes of thermokarst lakes at study sites, and vi) to address the effects of the long-term trends of hydro-climatic regimes and permafrost degradation on the areal changes of thermokarst lakes.

To accomplish these objectives, remotely sensed, field survey, and the reanalysis data were used in an integrated manner. Remote sensing data with spatial resolution 1.8-7.5 m (Corona panchromatic images), 15 m (Landsat ETM; band 8 panchromatic images), and 10 m (ALOS/AVNIR-2 images) were employed based on specific needs and their suitability for achieving the desired level of details. This study used remote sensing data from the 1962 to 2007 to investigate thermokarst lake changes at the study sites, so that thermokarst lake changes can be mapped over a relatively long period of time.

1.4. Outline of the thesis

This thesis contains six chapters. Chapter I describes the background information of thermokarst lakes and their importance, previous studies on thermokarst lakes, permafrost and thermokarst distributions in the study regions, research objectives, and outline of the thesis itself. Chapter II presents the geography, climate settings of the study region, and description of each study site.

Chapter III concentrates on the long-term hydro-climatic, and permafrost changes at the observation sites Mongolia, which follows the long-term reanalysis data and water balance model, and literature review on permafrost data. Chapter IV focuses on thermokarst lake dynamics at study sites in Mongolia from 1962 to 2007, which includes: the remote sensing images, the general methods for image processing and analyzing, mapping of thermokarst lakes, the areal changes on the categorized lake sizes, and volume changes of lakes in the continuous and isolated permafrost zones. In addition, the field survey include the ground control points, and remote sensing techniques, which has been recently used to orthorectify the high resolution Corona KH-4, KH-4A, and KH-4B, and ALOS/AVNIR-2 satellite data. Chapter V presented the general discussion on the thermokarst lake changes and lake size categorization in different permafrost zones, long-term climate and permafrost changes reflects on thermokarst lakes. Finally, Chapter VI presents the general conclusion of the study.

Chapter II. Physical settings of Mongolia

2.1. Topography and Vegetation

Mongolia is located in the central part of the Asia, and is bounded in the north by Russia and in the south by China. Topography of the country consists mainly of a plateau can, in general, be divided into the Altai, Hangai, Hovsgol, and Hentii mountains (Figure 2.1). The northwest and central parts are high mountain regions, while the eastern part is a vast steppe region. The southern part of the country is covered with semi-desert and desert area "Gobi desert" (MARCC, 2009). The average elevation of Mongolia is 1580 m above sea level (a.s.l). The bottoms of the lowest depressions are about 533 m a.s.l. while the highest of these is the Altai mountain region (up to 4000 m a.s.l) located in western Mongolia.

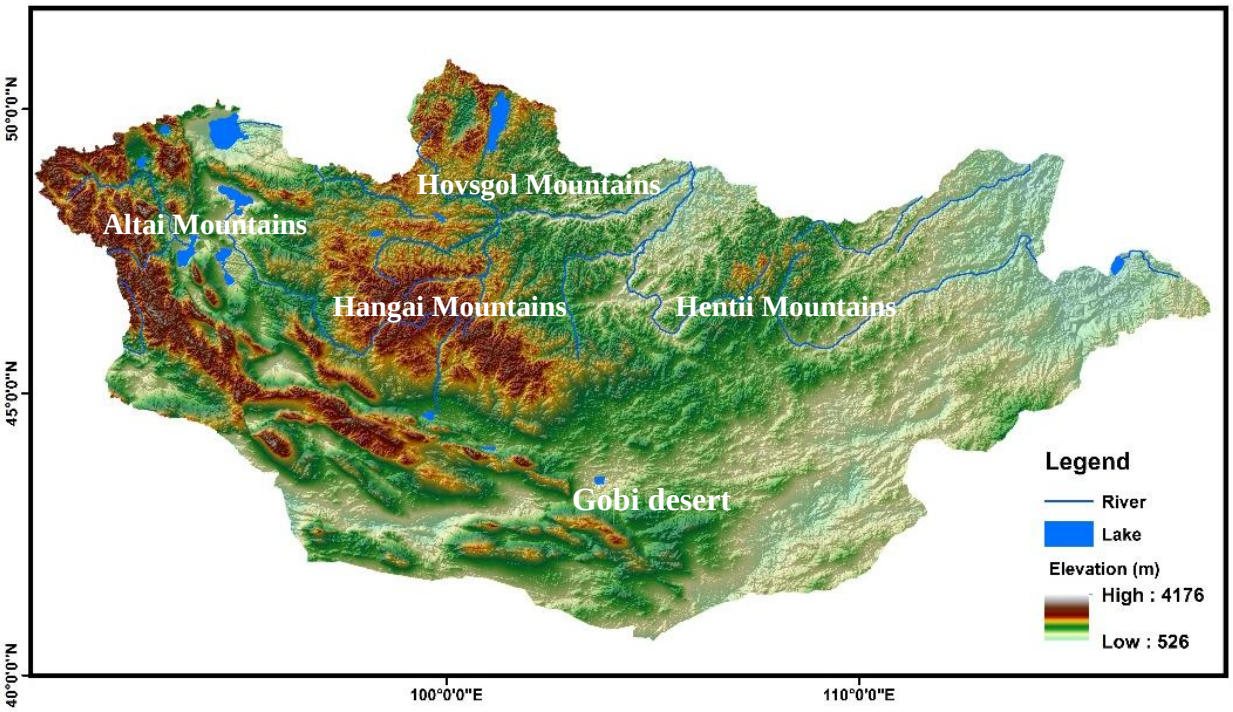

Figure 2.1. Topography of Mongolia

On the other hand, the territory of Mongolia has a transition zone in its rainfall amount as well as in its vegetation conditions, which change from desert to grassland and forest, over a north-to-south distance of only several hundreds of kilometers. In general, this transition zone is reflected in the vegetation patterns over Mongolia. The vegetation of Mongolia is characterized by Siberian forest, especially in the Hangai, Hentii, and Hovsgol mountains, and also by high mountain steppe vegetation in the Altai mountain region (Dorjsuren, 2014.).

2.2. Climate condition

Mongolia has a typically continental climate. A gradual temperature and moisture change is reflected in the prevailing climate pattern along a latitudinal gradient (MARCC, 2009). Climate of the country is characterized by, cold and moist conditions in the northern territories, warm and dry conditions in the southern territories. Winter air temperatures often reach to -50°C in the northern territory, and to 4°C in the south territory. In the warmest month, air temperatures range between 10 and 15°C in Hovsgol, Hangai, Altai, and Hentii mountains and reach up to 20°C in the southern province. The air temperatures are the lowest in mid-January and range between -25 and -30°C in the northern regions and between -15 and -20°C in the southern regions (Dagvadorj *et al.*, 2009). About 85% of total precipitation falls in warm season from April to September, of which about 60% falls between July and August (AIACC, 2005). Total annual mean precipitation is 300–400 mm in the Hangai, Hentii, and Hovsgol mountains, and it decreases to 100–200mm in southern Hangai and Altai mountains. Since 1940s, the precipitation over Mongolia has decreased at a rate of 0.1–2.0 mm per year, while the air temperature in Mongolia has increased by 2.14°C (Natsagdorj and Sarantuya, 2014).

2.3. Description of the study sites

In this study, seven sites are selected within the continuous and isolated permafrost zones of Mongolia (Figure 2.2-a): Darhad depression, Mungut river valley, Chuluut river valley, Khongor Ulun, Nalaikh depression, Galuut depression, and Erdene. These sites contain long-term permafrost monitoring boreholes located for our sites. Table 2.1 shows detailed information of basic hydro-climatology and environmental characteristics at all study sites. On the other hand, we collected ground control points (GCPs) at all study sites during the field work in 2009.

The Darkhad depression is located in the northern Hovsgol mountain region, within the ice-rich continuous permafrost zone (Table 2.1, Figure 2.2-a, and b). It is up to 40 km wide and 110 km long extended from north to south, is bounded by high mountains on all sides, which elevated up to 3300 m a.s.l (Figure 2.3-a). The depression has an extensive flat floor underlain by thick lacustrine sediments (Ishikawa and Jambaljav, 2015). Permafrost generally extends to depths of 150-200 m below ground in this depression, and the active layer ranges between 1–3 m depth (Sharkhuu, 2011). The mean annual ground temperature has been recorded as -3°C within the area (Ishikawa *et al*., 2012). The surface of the permafrost experienced strong thermal erosion, which resulted in the formation of thermokarst lakes on the depression floor during the Last Glacier Maximum (Krivonogov *et al*., 2012). Consequently, numerous thermokarst lakes concentrate in the depression floor. The depression is characterized by periglacial features including ice-wedge polygons, thermokarst, and frost mounds (Nishida and Jamsran, 2009; Tserensodnom, 2000; Tumurbaatar, 2001; Sharkhuu, 2011; Ishikawa and Jambaljav, 2015). The networks of ice-wedge polygons are only clearly visible at altitudes between 1560 and 1570m a.s.l. (Krivonogov *et al*., 2005), near the lacustrine terraces.

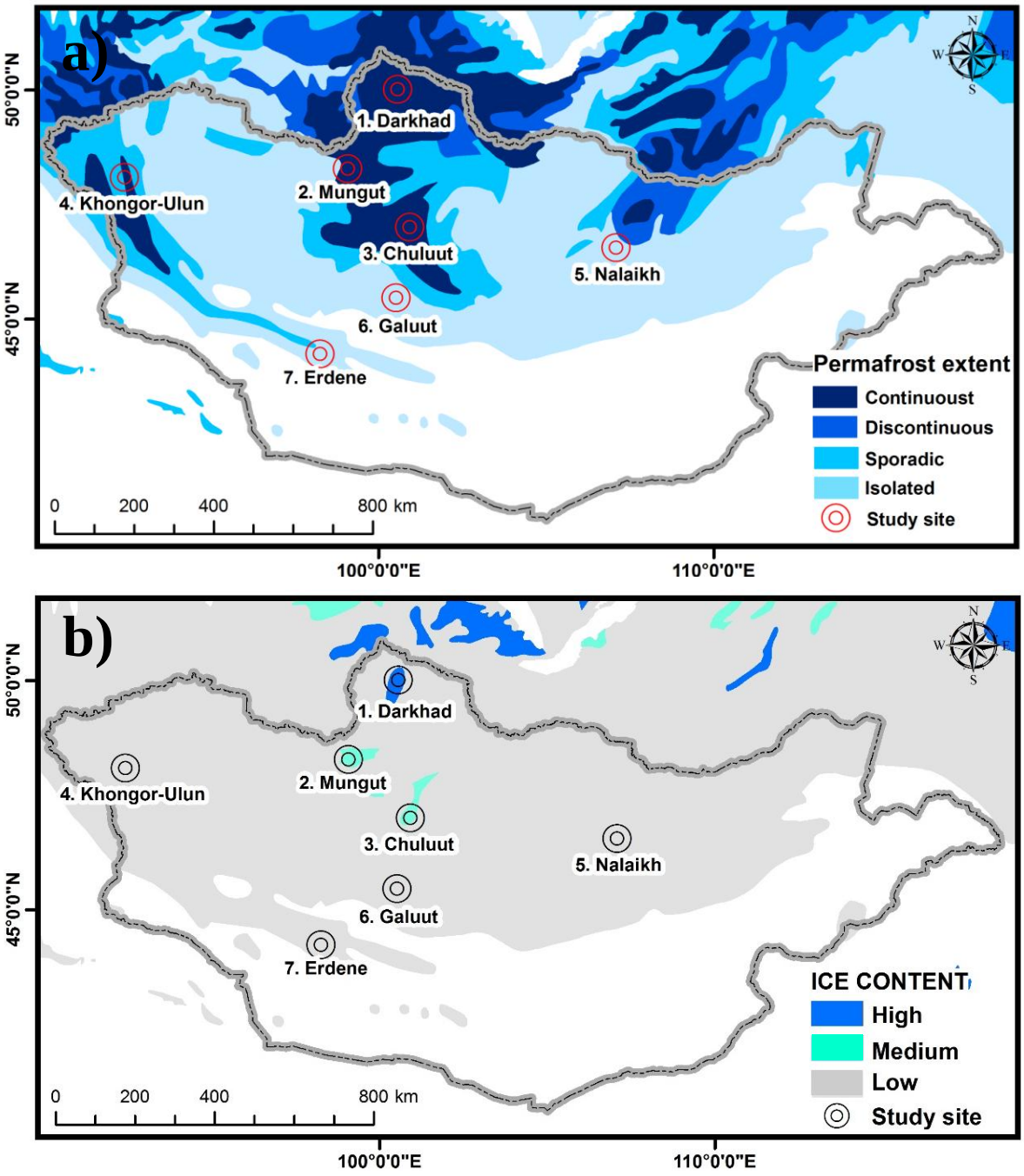

Figure 2.2. Location of study sites in different permafrost zones: a) Darkhad depression, Mungut river valley, Chuluut river valley, Khongor-Ulun, Nalaikh depression, Galuut depression, and Erdene. b) These study sites were located in different ice-content grounds.

The Mungut river valley is situated in the continuous permafrost with medium ice content, which is near the Hangain mountain region (Figure 2.2-a, and b; and Table 2.1). The entire the river valley was filled with lacustrine sediments during the Late Pleistocene (Yoshikawa *et al*., 2013). The sediment in the area is about 120 m thick, and permafrost is about 100 to 150 m thick, with a maximum depth of 200 m (Sharkhuu, 1969). Permafrost temperature at the site ranges from -1.2°C to -1.5°C, and the thickness of the active layer is 2.0–2.8 m (Sharkhuu, 2011; Ishikawa *et al*., 2012). The river valley is covered by small thermokarst lakes, pingos, and hummocks, surface characteristic shows clearly on Photo 2.1-b and Figure 2.3-b.

In the northern part of the Hangai mountain region, the Chuluut river valley is located in the continuous permafrost with medium ground ice content (Figure 2.2-a, and b). The valley is characterized by the inter-layering silt and clay sediments, permafrost thickness ranges from 15 m to 30 m (Sharkhuu, 1969). Permafrost temperature has been recorded as -1.6°C at the study site (Ishikawa *et al*., 2012), the active layer thickness ranges between 1.6 and 3 m (Jambaljav *et al*., 2013). Thermokarst processes have greatly influenced the landscaped in this area due to recent climate changes (Sharkhuu, 2011). Many small thermokarst lakes, pingo, and hummock exist along the river valley (Photo 2.1-c). On the other hand, the site is surrounded by larch forest on the northern slope of the mountains and by steppe grassland on the southern slope.

In the northwestern Altai mountain region, Khongor-Ulun is located within the high mountains, which elevated up to 3500 m a.s.l (Figure 2.3-d, and Photo 2.1-d). The permafrost temperature in this site, ranges between -2.4°C and -3.5°C, is colder than other study sites (Ishikawa *et al*., 2012). The study site in continuous permafrost is covered by several thermokarst lakes. These lakes probably formed as a result of permafrost degradation, which are connected to channel outflow (Tserensodnom, 2000).

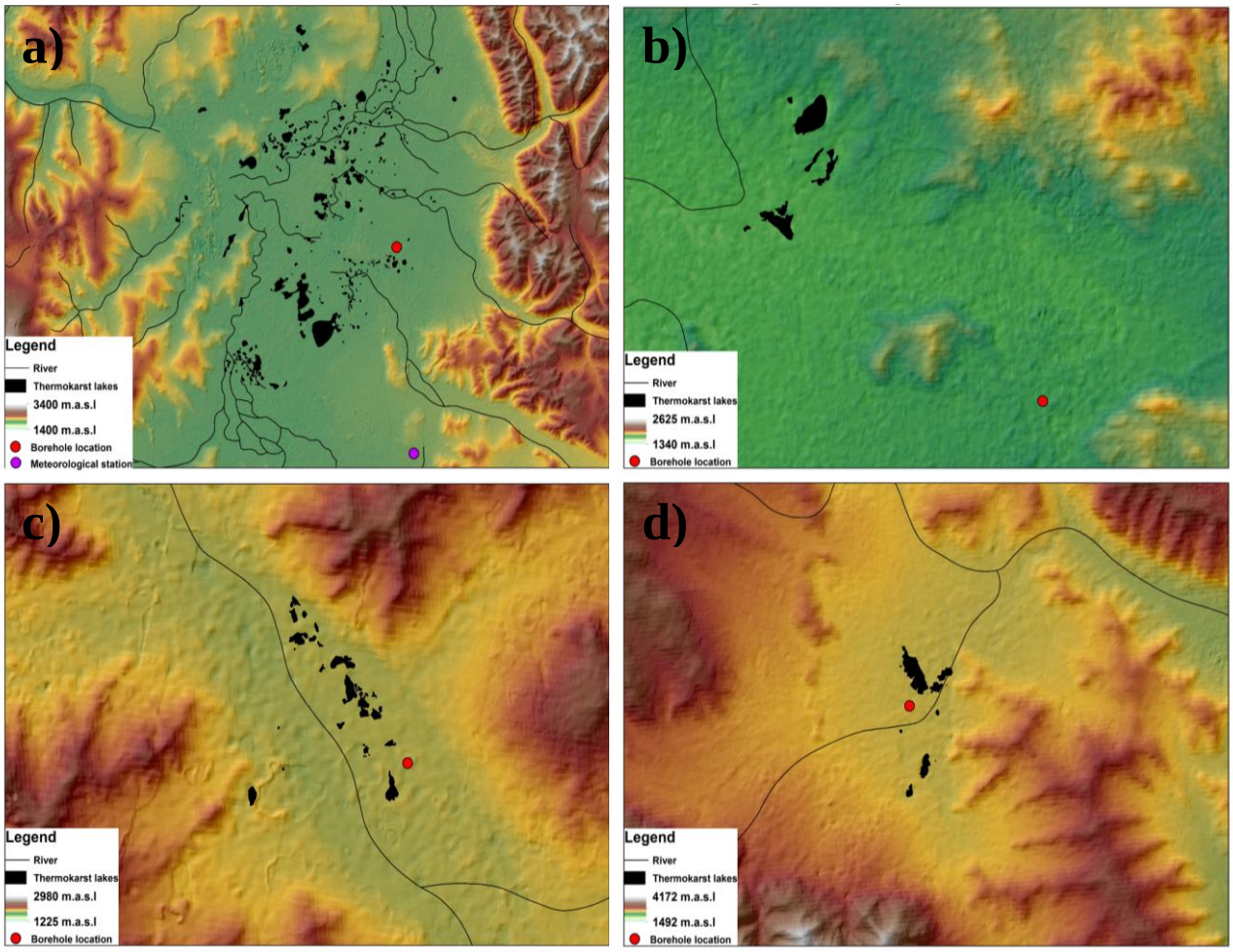

Figure 2.3. Topography map of study sites in the continuous permafrost zone: a) Darkhad depression, b) Mungut river valley, c) Chuluut river valley, and d) Khongor-Ulun. Black polygons represents surface area of the identified thermokarst lakes at these sites (as of 1962/1968).

We selected Nalaikh depression, Galuut depression, and Erdene in the isolated permafrost zone, and all of these sites are situated at the southern territory of Mongolia (Figure 2.2-a, and b). In the Hentii mountain region, the Nalaikh depression occupies on a flat semiarid pasture plain at 1421 m a.s.l (Figure 2.4-a). The extremely warm permafrost with the temperature at approximately -0.1°C was found (Ishikawa *et al*., 2012). The active layer with a depth of 7 m was under a dry condition at the site (Ishikawa *et al*., 2006). There are only two thermokarst lakes existed in center of this site (Photo 2.1-e, Figure 2.4-a). The territory of this site consists of sand and loam with some gravel (Wu *et al*., 2009).

Many small thermokarst lakes concentrate in the Galuut depression (Figure 2.4-b), the southern Hangai mountain regions (Tserensodnom, 2000). The depression is surrounded by high mountains with elevation up to 2500 m a.s.l, and is characterized by isolated permafrost with low ice content (Figure 2.2-a, and b). According to the permafrost monitoring studies, permafrost temperature is recorded by -1.0°C, and tick active layer found (Ishikawa *et al*., 2012; Jambaljav *et al*., 2013). The effects of thermo-erosion and thermokarst processes have degraded the surface characteristics of the site (Photo 2.1-f), which is one of the clearest examples of degradation of permafrost.

The Erdene is located in the southeastern Altai mountain region (Figure 2.2-a, and b), which is surrounded by arid-land high mountains (Figure 2.4-c), within the isolated permafrost zone. Few thermokarst lakes occupies in the area (Photo 2.1-g). Soil thawing temperatures have been recorded to depths of 8 m. According to in situ temperature measurements, the active layer thickness at the monitoring borehole site is more than 7.8 m, and permafrost temperature reaches -0.4°C (Ishikawa *et al*., 2012; Jambaljav *et al*., 2013).

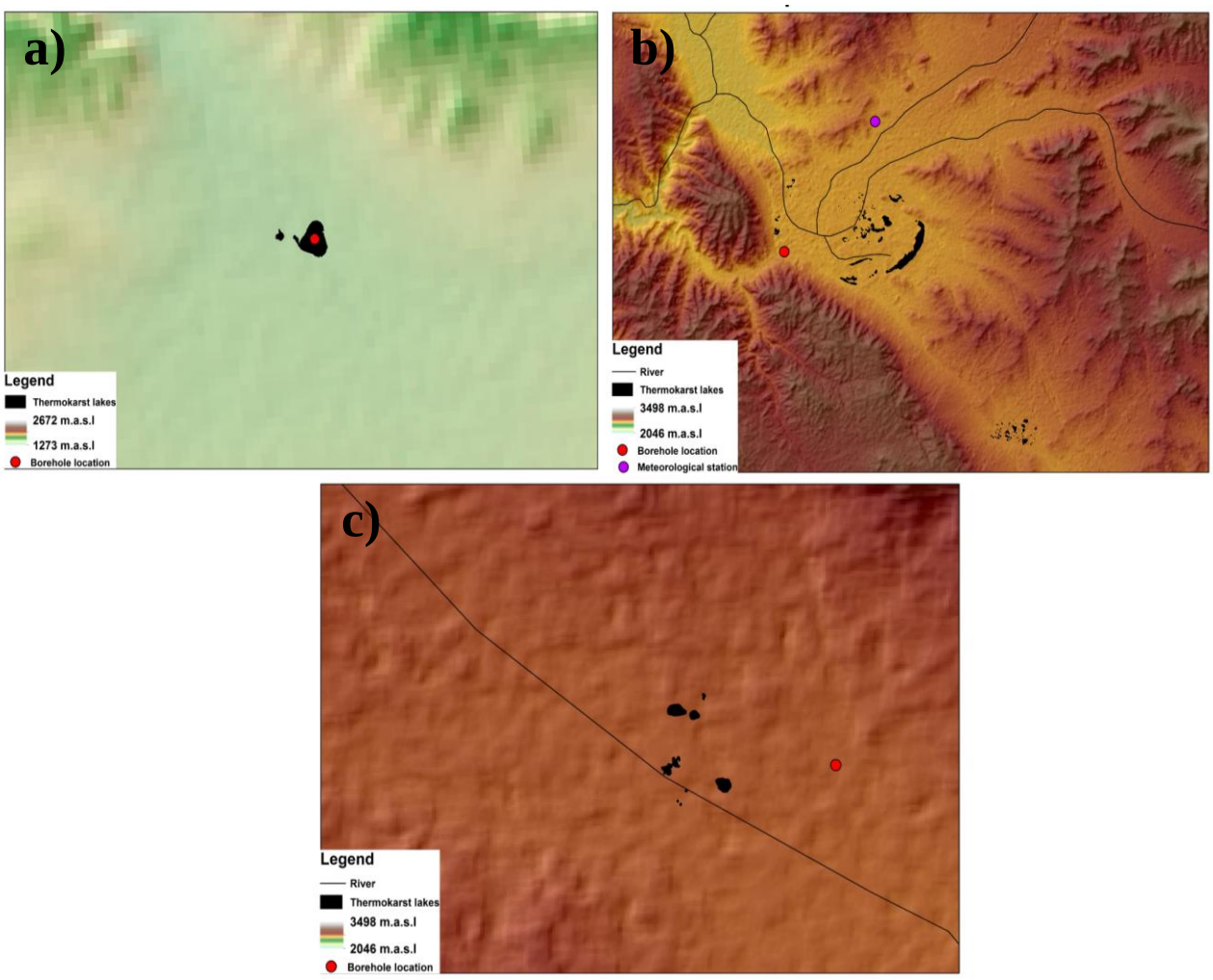

Figure 2.4. Topography map of study sites in the isolated permafrost zone: a) Nalaikh depression, b) Galuut depression, and c) Erdene. Black polygons represent surface area of the identified thermokarst lakes at these sites (as of 1962/1968).

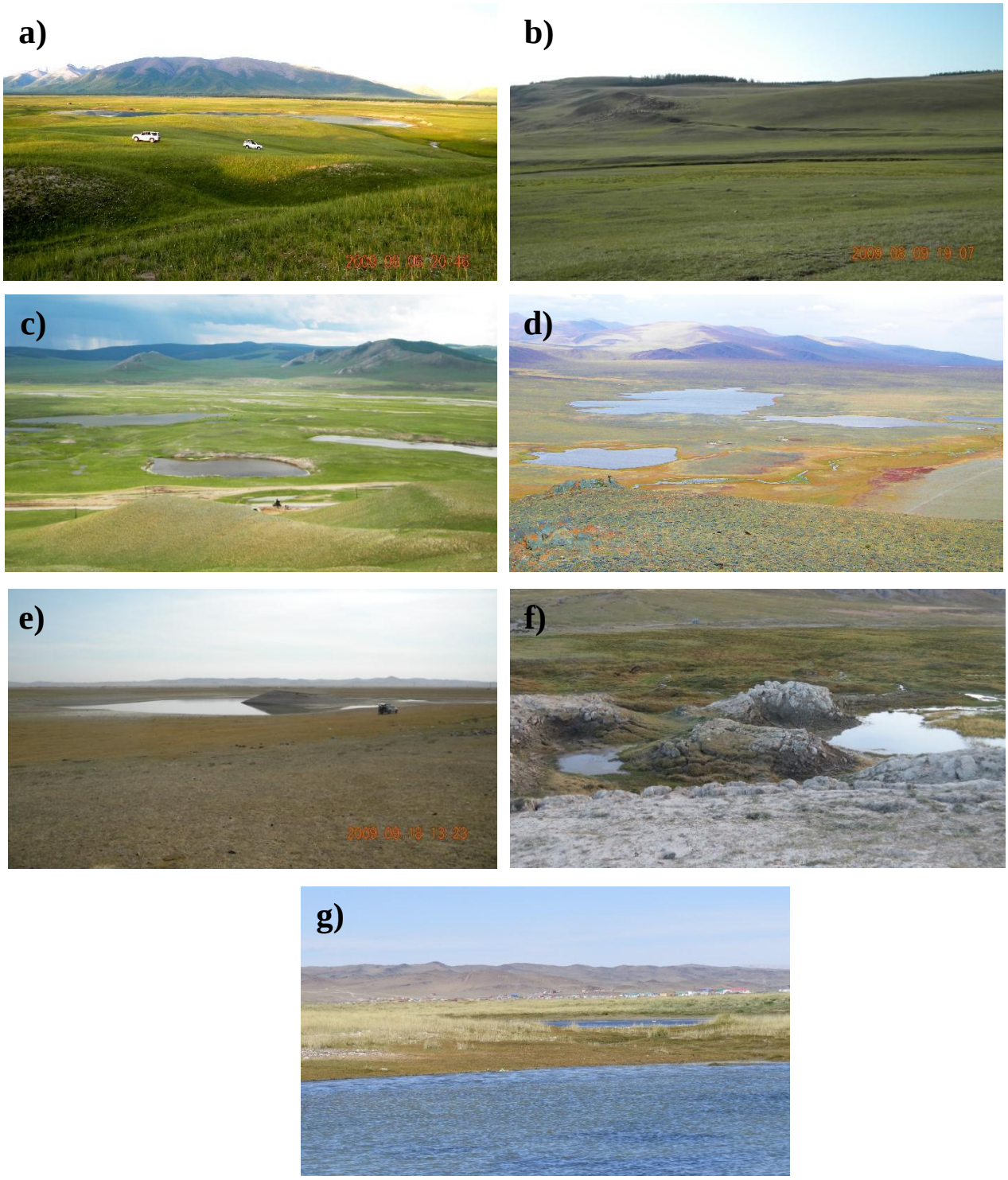

Photo 2.1. Surface characteristics of each study site: (a) Darkhad depression, (b) Mungut river valley, (c) Chuluut river valley, (d) Khongor-Ulun, (e) Nalaikh depression, (f) Galuut depression, and (g) Erdene. All photos were taken during the field work in 2009.

Table 2.1. General hydro-climatology and environmental characteristics at all study sites: Mean annual air temperature (MAAT/°C), summer air temperature (T/°C), mean annual precipitation (MAP/mm), and summer precipitation (P/mm) between 1962 and 2007 based on long-term reanalysis data. Permafrost and ground ice-content datasets at all study sites are updated from Brown *et al*., (1997). Ground control points (GCP) were collected from field work in 2009.

Study sites	**MAAT (°C)**	**Summer T (°C)**	**MAP (mm)**	**Summer P (mm)**	**Permafrost extent**	**Ice content**	**GCPs**
Darhad depression	-8.0	7.1	248	203	Continuous	> 20%	13
Mungut river valley	-6.4	8.0	199	153	Continuous	10-20%	5
Chuluut river valley	-6.3	8.7	229	185	Continuous	10-20%	11
Khongor - Ulun	-8.9	7.6	133	105	Continuous	0-10%	7
Nalaikh depression	-0.3	17.0	253	211	Isolated	0-10%	5
Galuut depression	-5.2	10.6	162	124	Isolated	0-10%	10
Erdene	-0.9	15.1	55	42	Isolated	0-10%	10

Chapter III. Climate and permafrost changes

3.1. Introduction

Climate changes can have an enormous influence on the distribution and state of permafrost (Brown and Pewe, 1973). It is the main factor controlling the formation and existence of permafrost. Although a general relationship exists between air and ground temperatures, local environmental factors play an important role on determining the permafrost distribution and its thermal regime. Recent climate warming in most northern high-latitude permafrost region has resulted in widespread warming of permafrost (IPCC, 2013), as proven by strong local evidence in Alaska, Siberia, Canada, and Central Asia (Smith *et al*., 2005; Romanovsky *et al*., 2010; Zhao *et al*., 2010). These studies have reported large spatial variations in warming rates in the northern hemisphere.

The climate of Mongolia is characterized by long and cold winters, short summers, small amount of precipitation, high temperature fluctuations (MARCC, 2014). Because of high altitude and latitude, it is generally colder than of other countries. The territory has a transition zone and mountainous regions, where that condition may change dramatically through short distances. These differences are exhibited clearly by our study sites in the region (see Figure 2.1 and Figure 2.2). Mongolia is extremely vulnerable, hence, to climate change due to its geographical location and environmental conditions. According to the observation data between 1940 and 2013 that the air temperature has increased by 2.07°C in the country (MARCC, 2014). This increase has occurred more intensively in the mountain regions and less so in the southern regions.

The permafrost occurring within the territory of Mongolia is significant different from permafrost in Alaska, in Canada, and in Siberian as a latitudinal permafrost and in Tibetan plateau (Davaa and Jambaljav, 2014). Permafrost in this country has temperatures close to 0°C and hence is highly vulnerable to climate warming due to its geographic location and permafrost extent (Ishikawa *et al*., 2012). Permafrost studies in this country have been conducted since 1950, however, continuous consistent measurements of permafrost temperature began mostly in last two decades. Monitoring of permafrost conditions has been conducted at numerous locations over the region at the southern fringe of Siberian permafrost region. Many studies have been published the thermal state of permafrost, active-layer depths, ground ice-content, and permafrost changes over Mongolian region (Brown *et al*., 1997; Sharkhuu *et al*., 2008, 2011; Ishikawa *et al*., 2012; Jambaljav *et al*., 2013, Davaa and Jambaljav, 2014). Due to climate warming, permafrost has not only been warming, but also disappearing, and the processes such as active layer detachment, deepening of summer thaw, disappearing of shallow permafrost have been determined (Davaa and Jambaljav, 2014). Overall, these studies have published suitable and sufficient data of permafrost thermal state, and its changes over Mongolia. Consequently, in this chapter, I obtained permafrost data at our study sites using the previously published articles.

The aim of this chapter is to present the two essential data sets such as climate and permafrost changes needed to evaluate the changes of thermokarst lake dynamics at our sites. The changes of lake area and numbers are due to several potential processes, including (1) changes in precipitation, (2) changes in air temperature and evapotranspiration, (3) water balance, and (4) changes in permafrost conditions such as subsurface drainage, ground ice content, and active layers.

3.2. Data and methods

Systematic meteorological observations began in the early 1940s. However, Mongolia has a sparse distribution of meteorological stations with weather records spanning more than 50 year; therefore, we used the reanalysis data in this study. The mean annual air temperature (MAAT), maximum and minimum air temperatures at 2 meter height data from 1962 to 2007 were downloaded for the National Center for Environmental Prediction, National Center for Atmospheric Research (NCEP/NCAR) data (Kanlay *et al*., 1996). The horizontal resolutions of the compiled NCEP/NCAR precipitation datasets (2.5˚ × 2.5˚) were not sufficient to investigate rainfall. Therefore, the annual total precipitation (P) was downloaded from the high-resolution Asian Precipitation Highly Resolved Observational Data Integration Towards Evaluation (APHRODITE) data with 0.5˚ × 0.5˚ resolution from 1962 to 2007 (Yatagai *et al*., 2009). In addition, that the APHRODITE data is available until 2007. Therefore, we only used satellite images from 1962 to 2007. Both reanalysis NCEP/NCAR and APHRODITE data were analyzed in the Grid Analysis and Display System (GrADS) software.

On the other hand, this study used seven meteorological stations (e.g., Renchinkhlumbe, Numrug, Terkh, Bayan-Ulgii, Ulaanbaatar, Galuut, and Gobi-Altai) for air temperature, and precipitation (1979 to 2007), which are needed to validate the reanalysis data at all study sites. These meteorological station data were obtained from Institute of Meteorology and Hydrological in Mongolia. In addition, only two meteorological stations occupied at our study sites such as the Darkhad and Galuut depressions. Other study sites are located so far from the stations, which are distance from 50 to 150 km.

3.3. Description of water balance model

To estimate water balance, we calculated annual potential evapotranspiration (PET) using the Thornthwaite's water balance model (McCabe *et al*., 2007). This water balance model (Figure 3.1) analyses the allocation of water among various components of the hydrologic system using a monthly accounting procedure based on the methodology originally presented by Thornthwaite (Thornthwaite, 1948). Inputs to the model are monthly maximum and minimum air temperatures (T°C), monthly total precipitation (P, mm), and the latitude (in decimal degrees) of the study site location. The latitude of the location is used for the computation of day length, which is needed for the computation of potential evapotranspiration (PET). Finally, we estimated water balance by subtracting P from PET (P-PET) for the study period of 1962 and 2007.

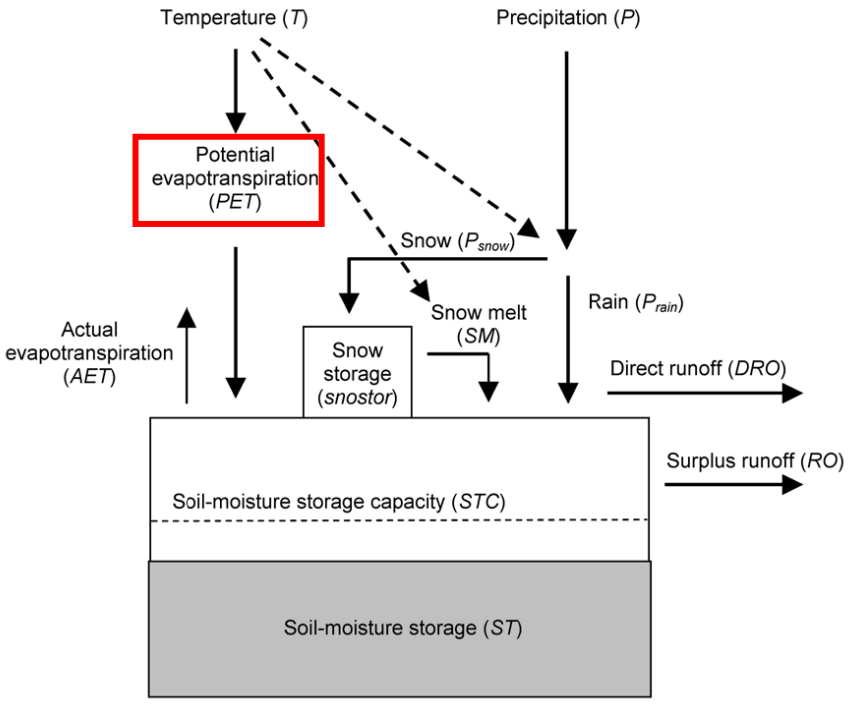

Figure 3.1. Diagram of the Thornthwaite water balance model (McCabe *et al*., 2007).

3.4. Results and Discussions

3.4.1. Data validation

Figures 3.2 showed correlation between the reanalysis data and observation data for (a) the mean annual air temperature and (b) total annual precipitation between 1979 and 2007. As shown the results in the mean annual air temperature (Figure 3.2-a), correlation between NCEP/NCAR and station data demonstrated good correlations demonstrated in the Darkhad depression ($r^2=0.67$), Mungut river valley ($r^2=0.63$), Chuluut river valley ($r^2=0.75$), and Khongor-Ulun ($r^2=0.52$). These results were depending on distance between our study sites and meteorological stations. Therefore, we did not interest absolute values, but focused only on their trends.

Considering the graphic of the trends (Figure 3.2-b), we employed the APHRODITE data for total annual precipitation. Their trends showed good correlations in the Dakhad depression and Chuluut river valley ($r^2 =0.77\text{-}0.82$). However, the insignificant correlations were observed in the Mungut river valley, and Khongor-Ulun. Because, these sites are located so far from the meteorological stations (approximately 100-150 km).

In the Nalaikh depression, the correlations showed good trends ($r^2 =0.71$, $r^2 =0.60$) for air temperature and precipitation, respectively (Figure 3.3-a). This site located near to the meteorological station. However, in the Galuut depression, and Erdene, the correlations between NCEP/NCAR, APHRODITE, and observation data for temperature and precipitations were represents sparse. One of the potential factor is likely consistent with the distances between study sites and meteorological stations.

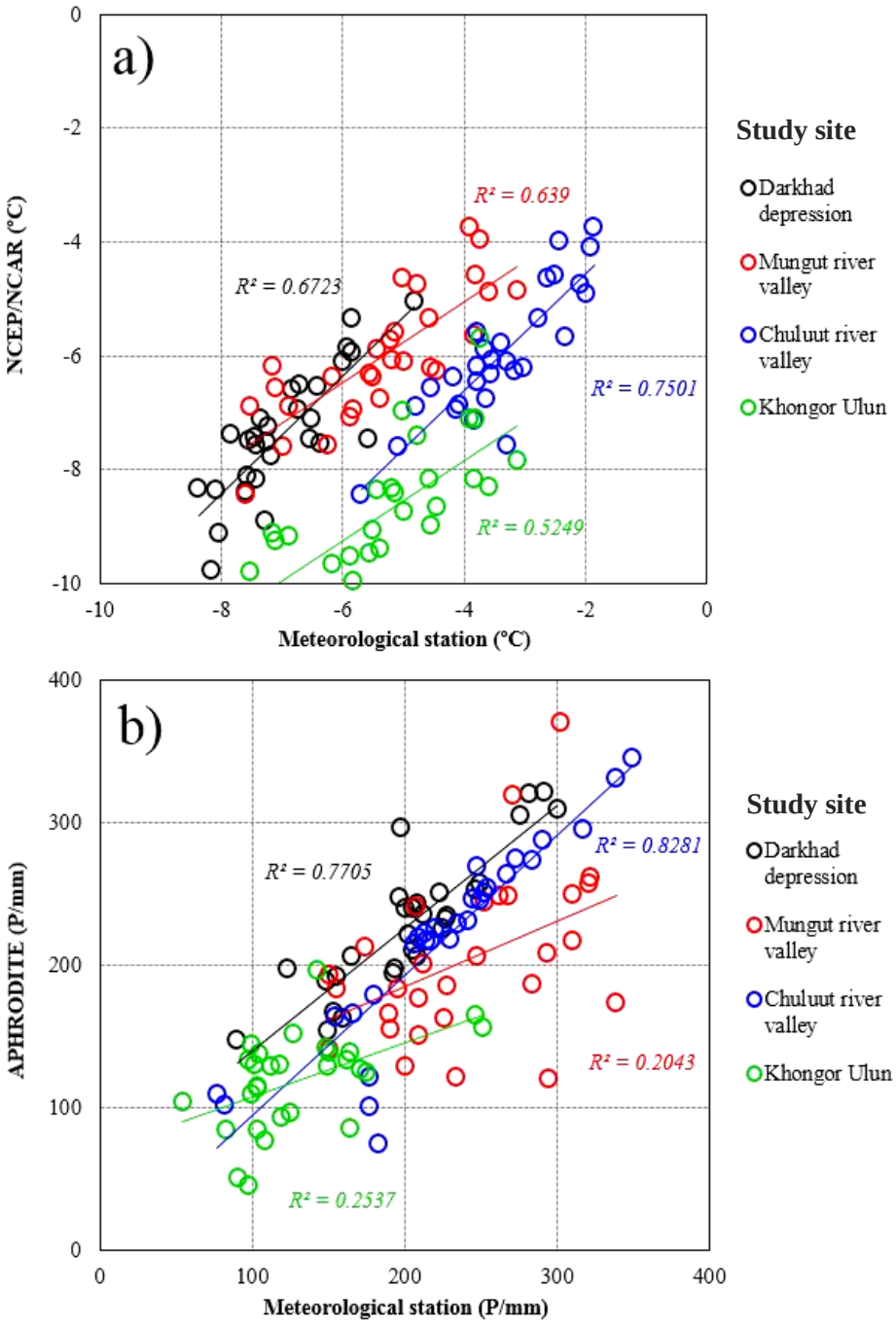

Figure 3.2. Scatterplots of the reanalysis data (NCEP/NCAR & APHRODITE), and observation data such as Renchinkhlumbe, Numrug, Terkh, and Bayan-Ulgii from 1979 to 2007 in the continuous permafrost zone: a) NCEP/NCAR and observation data for MAAT (C°), and b) APHRODITE and station data for total annual P (mm).

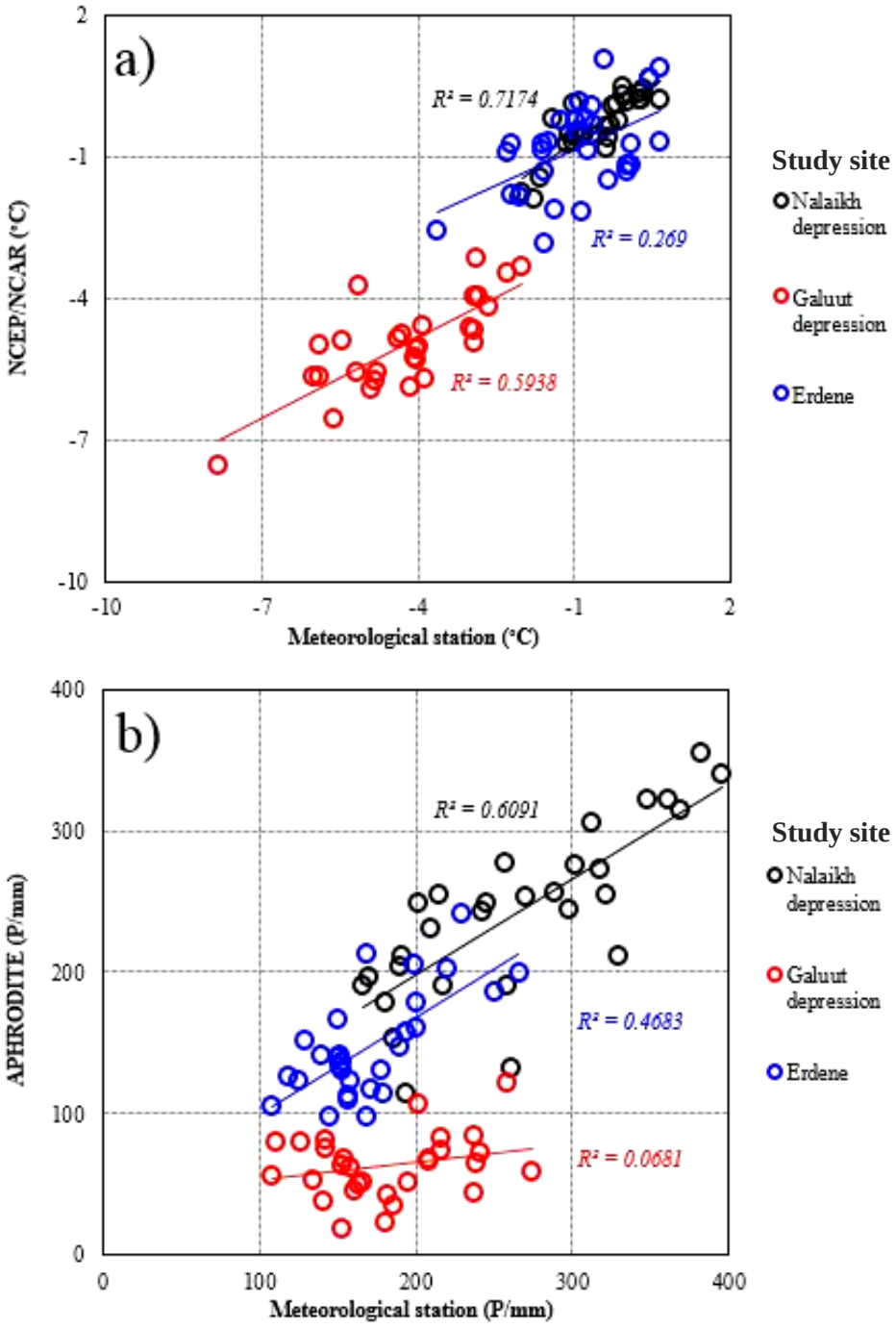

Figure 3.3. Scatterplots of the reanalysis data, and meteorological station data such as Ulaanbaatar, Galuut, and Erdene from 1979 to 2007 in the isolated permafrost zone: a) NCEP/NCAR and station data for MAAT (C°), and b) APHRODITE and station data for total annual P (mm).

3.4.2. Hydro-climatic changes

Figure 3.4 illustrates the hydro-climatic change trends derived from the reanalysis data at study sites in the continuous permafrost zone. Their statistics analysis such as changes (Δ) between 1962 and 2007, correlation coefficient (r^2), and significance level (p) are demonstrated in Table 3.1. During the last 45 years, we found significant linear increasing trends in MAAT at the Darkhad depression, Mungut and Chuluut river valleys, except Khongor-Ulun (Figure 3.4-a). The Khongor-Ulun occupies in the cold and high mountains regions, which was probably correlated with lower changes than other sites (Table 3.1). Particularly these trends were increased rapidly since 1980. Due to the rising air temperatures, trends in total annual PET have also increased significantly (Figure 3.4-c). However, trends in total annual P were not changed any significant trends, while water balance observed negative trends at all sites (Figure 3.4-d). The above mentioned study sites are located in the northern territory of Mongolia as linear transect (see Figure 2.2), there were hydro-climatic variations ranged more than Khongor-Ulun.

Conversely, in the isolated permafrost zone, the hydro-climatic change trends at Nalaikh depression, Galuut depression, and Erdene were carried out for all parameters (Figure 3.5). In these sites, long-term trends for MAAT increased slightly during the last 45 years, expect Erdene (Figure 3.5-a). According to these result, their trends in the total annual PET were increased slowly (Figure 3.5-c). The trends of total annual P were observed at both Nalaikh and Galuut depressions without any significant trends; however it increased at Erdene (Figure 3.5-b). There were observed opposite trends with insignificant correlations in water balance (Figure 3.5-d, Table 3.1). For example, trends of MAAT and P almost no changed at Erdene. These differences may attribute to the large attitudinal climatic gradient in Mongolia.

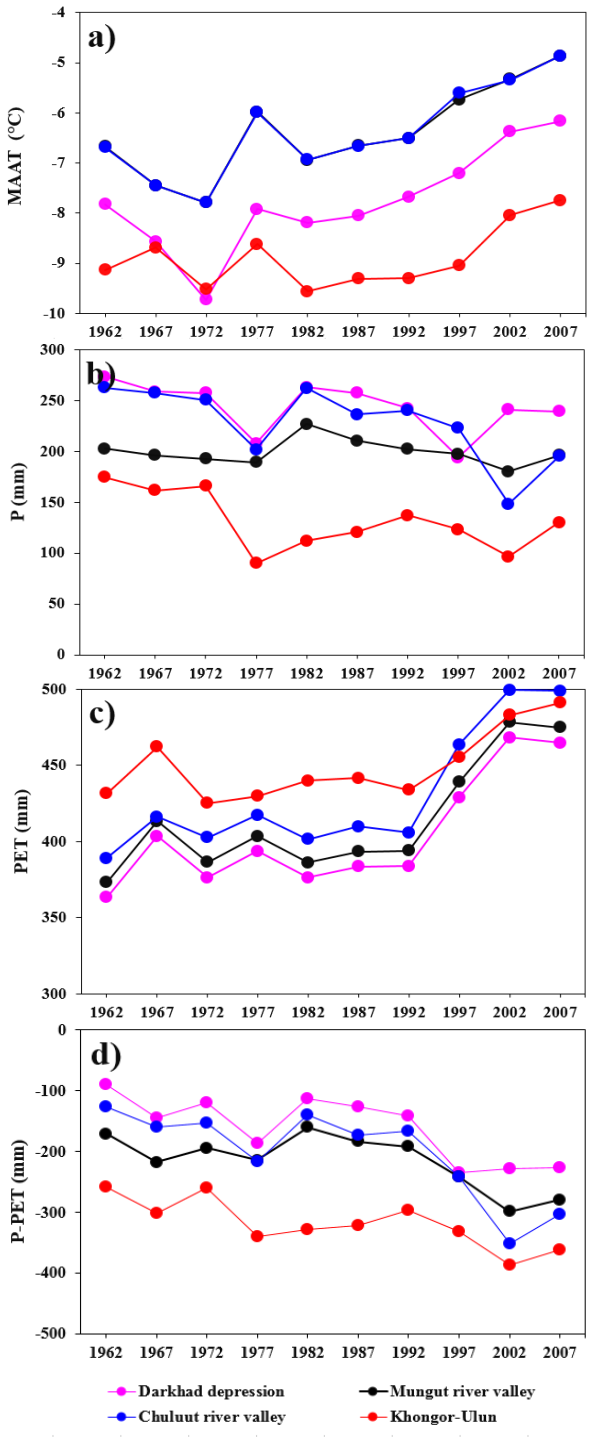

Figure 3.4. Hydro-climatic change trends (5-years moving average) at Darkhad, Mungut river valley, Chuluut river valley, and Khongor-Ulun in the continuous permafrost zone from 1962 to 2007: a) mean annual air temperature (MAAT), b) total annual precipitation (P), c) total annual potential evapotranspiration (PET), and d) water balance (P-PET).

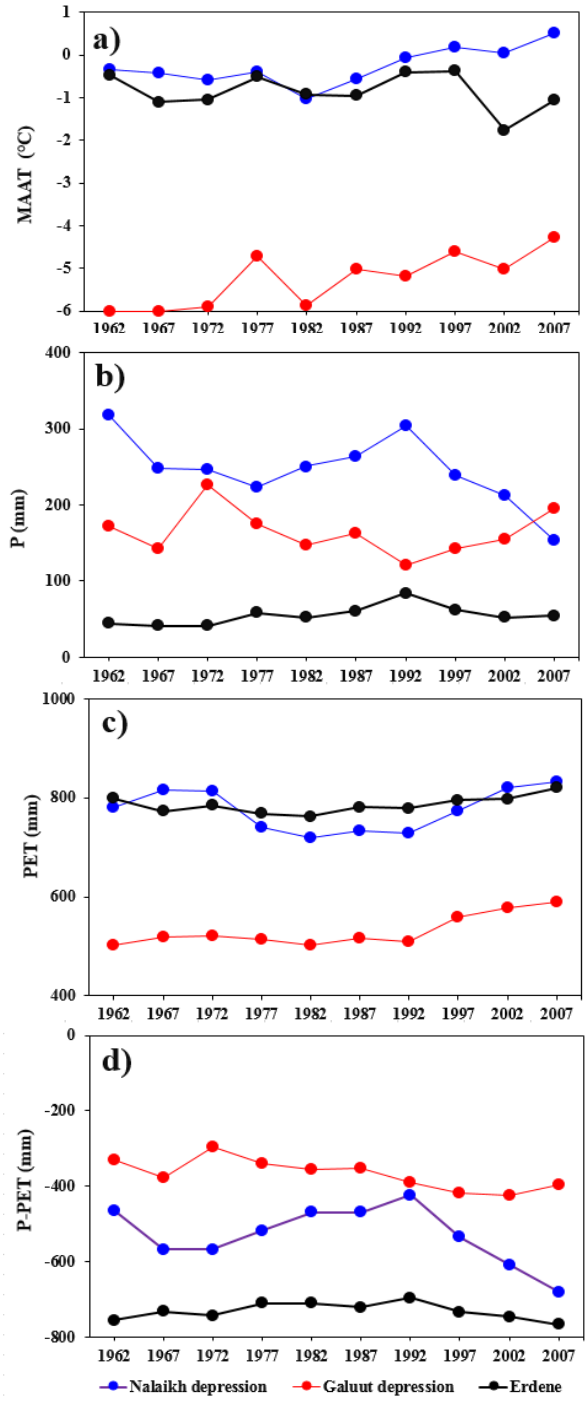

Figure 3.5. Hydro-climatic change trends (5-years moving average) at Nalaikh depression, Galuut depression, and Erdene in the isolated permafrost zone from 1962 to 2007: a) mean annual air temperature (MAAT), b) total annual precipitation (P), c) total annual potential evapotranspiration (PET), and d) water balance (P-PET).

Table 3.1. Linear trends in mean annual air temperature (MAAT), total annual precipitation (P), total annual potential evapotranspiration (PET), and water balance (P-PET). Their statistical parameters were computed such as changes (Δ) between 1962 and 2007, coefficients of determination of the liner trend (r^2) and significance level (p).

Study sites	MAAT (°C)			Total Annual P (mm)			Total Annual PET (mm)			Water Balance (P-PET) (mm)		
	Δ	r^2	p	Δ	r^2	p	Δ	r^2	p	Δ	r^2	p
Darkhad depression	2.65	0.33	0.001	-13.4	0.00	0.443	81.5	0.41	0.001	-94.9	0.17	0.001
Mungut river valley	2.34	0.32	0.001	-14.9	0.00	0.651	81.6	0.41	0.001	-96.5	0.16	0.001
Chuluut river valley	2.39	0.33	0.001	-100.5	0.21	0.006	94.9	0.47	0.001	-195.4	0.40	0.001
Khongor-Ulun	0.79	0.05	0.034	-41.5	0.03	0.044	37.8	0.13	0.001	-79.3	0.09	0.003
Nalaikh depression	0.91	0.15	0.011	-49.1	0.06	0.007	4.63	0.00	0.721	-53.7	0.03	0.049
Galuut depression	1.62	0.23	0.001	-32.3	0.04	0.076	66.1	0.29	0.001	-98.4	0.24	0.001
Erdene	0.35	0.01	0.322	+27.8	0.13	0.017	14.6	0.01	0.093	+13.2	0.00	0.859

3.4.3. Spatial pattern of the mean annual air temperature and precipitation

The differences in the MAAT (from NCEP/NCAR data) over Mongolia between 1962 and 2007 illustrates in Figure 3.6. As shown the results, it was colder temperature in the west and northern parts than southern parts of Mongolia during the first decadal (1962 to 1972). Next two decades, these spatial patterns are increased over the territory. During the last decade, it has increased dramatically in the north and center parts of Mongolia. Furthermore, this increase has occurred more intensively at Darkhad depression, Mungut and Chuluut river valleys in the continuous permafrost zones within the Hovsgol, Hangai, and Altai mountain regions (Figure 2.2). However, in southern territories, it was decreased in last decades. These patterns were typically consisted with previous studies. According to study of climate changes over Mongolia (Natsagdorj and Sarantuya, 2014), the mean annual air temperature has increased significantly since 1940s.

On the other hand, Figure 3.7 shows the difference in the total annual precipitation (P) over the study region, which extracted from APHRODITE data. In general, the precipitation pattern for 1962-1972 was wetter in northern and eastern parts than the west and southern parts of the territories. Two decades between the 1972-1982 and 1982-1992, the plot shows that the smoothly decreases in the north and eastern parts of Mongolia. In last decade, the significant negative spatial pattern observed over the territory, which occupied especially in the central and eastern parts. Our results are consistent with historical observations. For example, the Mongolia Second Assessment Report on Climate Change (MARCC, 2014) published the total annual precipitation changes over Mongolia. This report summarized that the precipitation has decreased year to year.

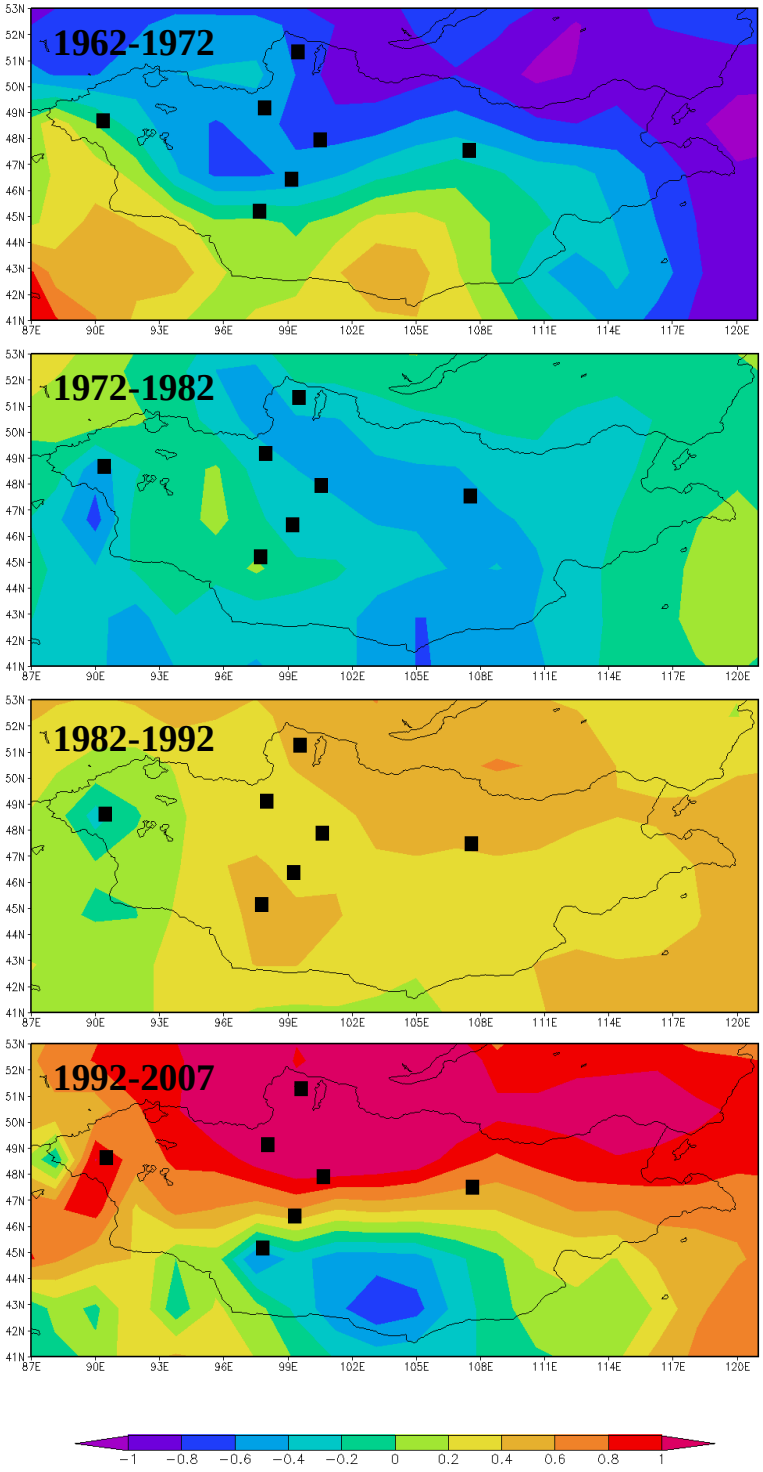

Figure 3.6. The differences in the mean annual air temperature (MAAT, °C) during the last four decades in Mongolia based on the NCEP/NCAR data. Black points indicate the position of all study sites.

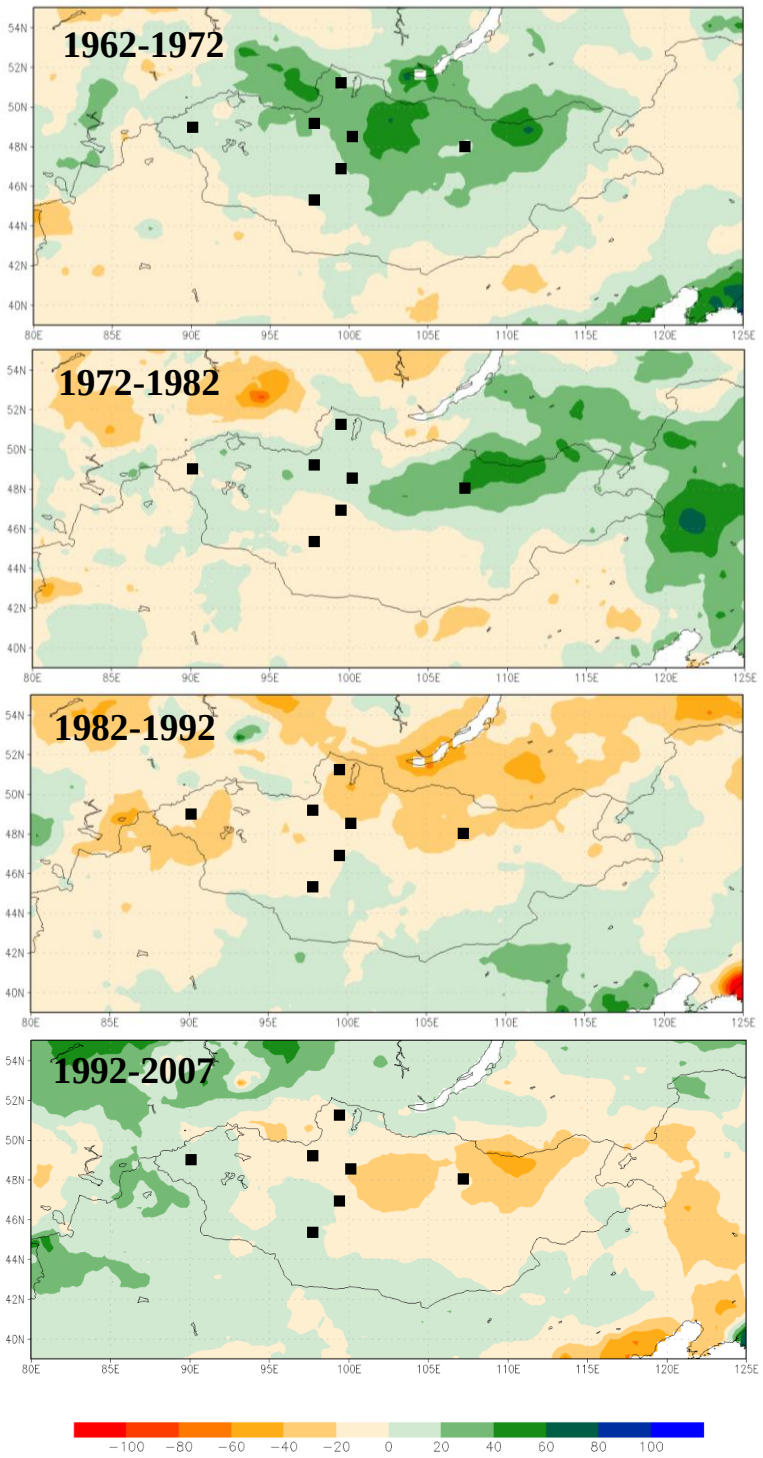

Figure 3.7. The differences in the total annual precipitation (P, mm) during the last four decades in Mongolia based on the APHRODITE data. Black points indicate the position of all study sites.

3.4.4. Permafrost changes in Mongolia

Many studies have reported permafrost changes in Mongolia, the southern fringe of Siberian permafrost region. Most of these studies identified that permafrost has degrading due to climate change. For example, at the Darkhad depression in the northern Hovsgol mountain region, permafrost temperature has increased by 0.95°C at a depth of 10-15m during the last 23-26 years (Figure 3.8) (Bat-Erdene, 1995; Jambaljav *et al*., 2013). In northern Hangai mountain region, the temperatures at a depth of 10-15m have been warmed by 0.39°C-0.44°C at the Chuluut river valley and Mungut river valley during the last 24 years (Jambaljav *et al*., 2013). The temperature at the depth of 10m has been warmed by 0.38°C during the last 23 years at the Tsagaan nuur in the northern Altai mountain region, which is near to our study site with the Khongor-Ulun. In contrast, at the Nalaikh depression, the temperature is raised insignificantly by 0.02°C (Sharkhuu, 2011). The temperature at a depth of 10 m has increased by 0.64°C for the last 30 years in Galuut depression (Davaa and Jambaljav, 2014). While the temperature at a depth of 8m has increased insignificantly about 0.1°C for last 30 years in Altai mountain region, which is extended on the southern fringe of the Mongolian permafrost region. However, according to in-suite temperature measurements, permafrost temperatures have increased insignificantly at the Nalaikh depression and Erdene (Figure 3.8). According to these results, in the continuous permafrost in northern Mongolia has warmed faster than southern isolated permafrost zone over recent decades, there were detachments of active layers, deepening of summer thaw, disappearing of permafrost in the southern territory of Mongolia (Sharkhuu *et al*., 2008 and 2011; Ishikawa *et al*., 2012; Jambaljav *et al*., 2013). On the other hand, these results of permafrost changes at study sites are consistent with our analysis in climate changes.

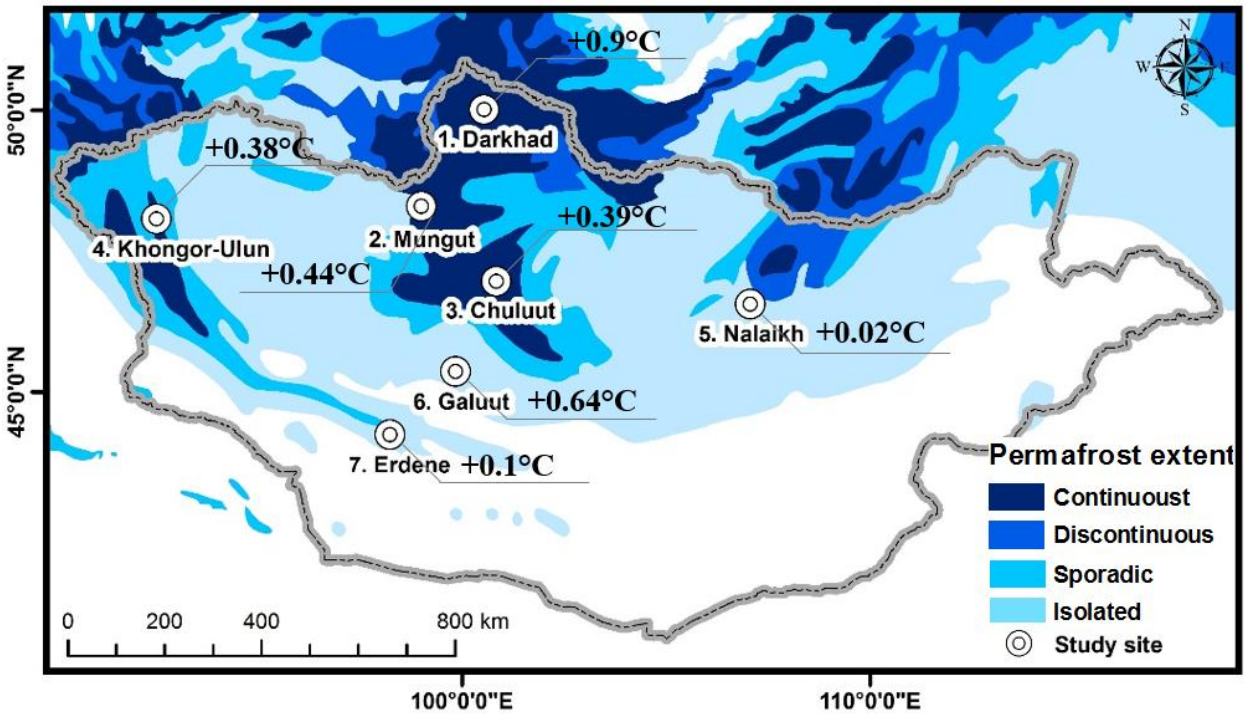

Figure 3.8. Permafrost changes at study sites in Mongolia from 1973 to 2009.

3.5. Conclusion

This study examined the climate and permafrost changes at seven study sites using long-term reanalysis data and article review for permafrost data. The main conclusions of this chapter are as follows:

1. During the last decade, mean annual air temperature and potential evapotranspiration have increased dramatically in the north and center parts of Mongolia. This increase has occurred more intensively at Darkhad depression, Mungut and Chuluut river valleys in the continuous permafrost zones within the Hovsgol, Hangai, and Altai mountain regions. However, such parameters were increased slightly in the southern isolated permafrost. These patterns might have correlated to higher latitude gradients. On the other hand, this study observed the negative water balance at all sites during the same period, except a site (Erdene).

2. According to previous studies on permafrost, it is temperature increased at all study sites, especially northern continuous permafrost zone (Darkhad deoression, Mungur, and Chuluut river valleys). Recent degradation of permafrost in Mongolia is almost similar to with other permafrost regions.

Chapter IV. Thermokarst lake changes in the continuous and isolated permafrost zones from 1962 to 2007

4.1 Introduction

Thermokarst lake is one of the most obvious form of permafrost degradation in the northern hemisphere (Morgenstren *et al*., 2011). Recently, northern permafrost regions are dotted with tens of thousands of thermokarst lakes (Grosse *et al*., 2013). Thermokarst lakes have their largest distribution in Arctic and sub-Arctic regions with ice-rich unconsolidated sediments, poorly consolidated and ice-rich bedrock, and mountain valleys (Figure 4.1). They strongly influence the surface energy balance in permafrost regions with feedbacks on the ground thermal regime (Jorgenson *et al*., 2010). Thus, the lateral and vertical dynamics of thermokarst lake change result in complex interactions with topography, stream, neighboring lakes, and permafrost (Jones *et al*., 2011). Given current climate change it is important to conduct studies on thermokarst lake dynamics as they are through to be indicator of the climate change on the permafrost landscape.

A suite of recent studies have utilized remotely sensed imagery to document changes in thermokarst lake extent in various locations across the Arctic and sub-Arctic. Long-term thermokarst lake dynamics in Canada and Alaska suggest that the inter-annual variation in precipitation is the dominant driver of surface area extent (Plug *et al*., 2008). Inter-annual variation in lake evaporation is generally less than precipitation, although recent trends in the duration of open water season due to earlier ice-out suggest potentially increasing summer evaporative losses from lakes (Labrecque *et al*., 2009). Since thermokarst lakes develop and

expand through degradation of surface permafrost, much interest exists in how these lakes are changing with amplified climate warming. In a remote-sensing study, Smith *et al*. (2005) analyzed lake change between 1973 and 1997–98 and found that thermokarst lakes in Siberia increased in surface area extent and number in the continuous permafrost zone, which was attributed to lake expansion through shoreline erosion. However, lake area and number decreased in the discontinuous to isolated permafrost zones, which was attributed to the penetration of taliks and subsurface drainage. This mechanism of thermokarst lake drainage has also been documented in Alaska, detailing lake-groundwater connectivity and vertical hydraulic gradients for a discontinuous permafrost environment (Yoshikawa and Hinzman, 2003). Riordan *et al*. (2006) found dramatic trends of thermokarst lake shrinkage in the discontinuous permafrost zone in Alaska and attributed these changes to increasing evapotranspiration.

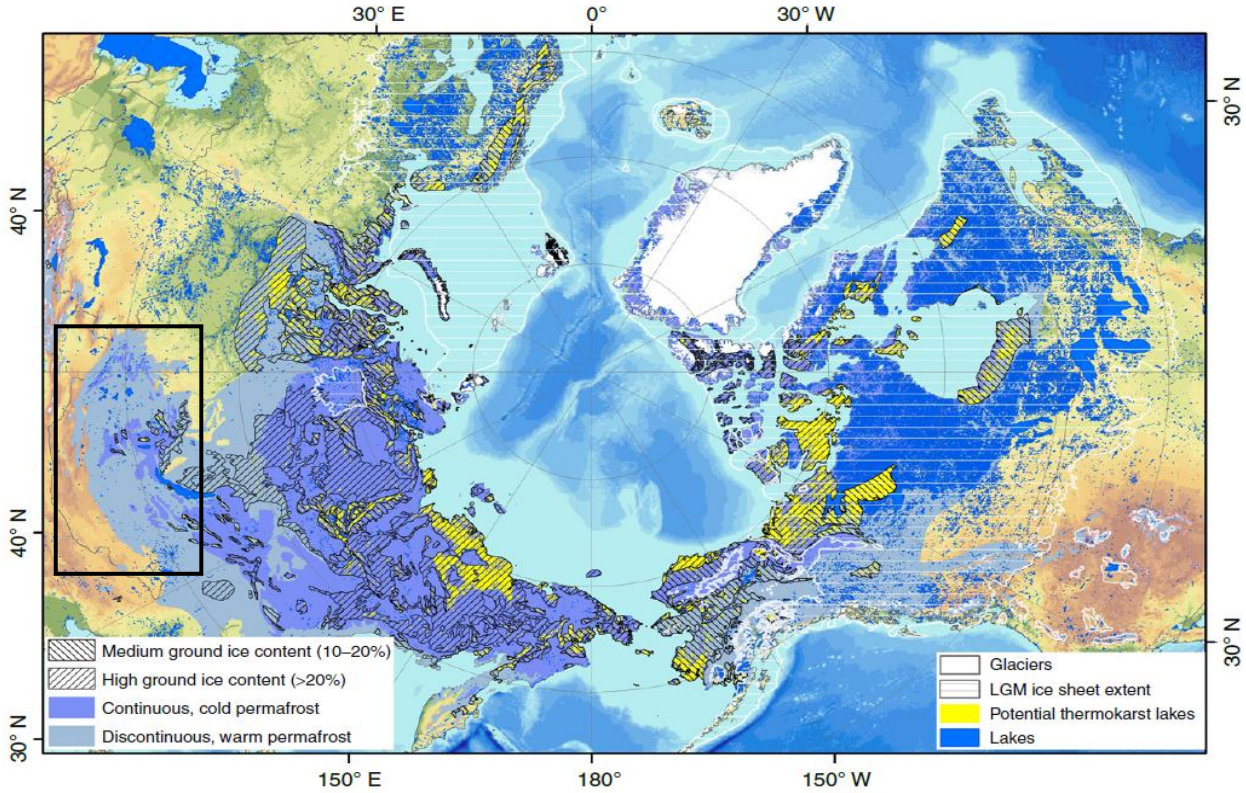

Figure 4.1. Arctic and sub-Arctic map showing probable thermokarst lake regions (map compiled by Grosse *et al*., 2013). Black rectangle represents location of study region.

A similar geographical shift of permafrost zones from continuous in northern territories to sporadic in the southern region is seen in Mongolia. In addition, climatic gradients occur along latitude as well; it is, colder and wetter in the northern territory, and warmer and drier in the southern territory. Although this environmental gradient would be interesting for comprehensive analysis of the factors controlling dynamics of thermokarst lakes, which have extensively developed on the depressions and valleys in the Altai, Hangai, Hovsgol and Hentii Mountain regions (Tserensodnom, 2000; Tumurbaatar, 2001; Nishida and Jamsran, 2009), the spatiotemporal changes of these lakes have not been investigated in Mongolia so far.

This chapter focuses on the thermokarst lake dynamics at seven study sites in different permafrost zones of Mongolia, where numerous thermokarst lakes exist on the depressions and valleys within the various mountain regions. First objective of this chapter is to provide quantitative information on the temporal and spatial changes of thermokarst lakes in Mongolia using a time series of high-resolution satellite imagery. Second objective is to categorize the extracted lake areas into four distinct classes in order to better understand the lake dynamics of individual lake size categories. Last objective is to calculate water volume changes of thermokarst lakes at two depressions, where numerous thermokarst lakes concentrate. High resolution satellite imagery, digital elevation model, and field measurements were employed for these objectives during long-term time period.

4.2. Remote sensing datasets

In this study, we used satellite imagery to identify areal extent of thermokarst lakes at study sites for three different time series: 1962-1968, 1999-2001 and 2006-2007. All images were acquired during the summer season. For this analysis we employed 14 Corona scenes, 7 Landsat Enhanced Thematic Mapper Plus (ETM+) images, and 7 Advanced Land Observing Satellite (ALOS) Advanced Visible and Near Infrared Radiometer type 2 (AVNIR-2) satellite data sets. The detail information of these satellite datasets are illustrated in Table 4.1.

Table 4.1. The Corona KH-4, KH-4A, and KH-4B, Landsat ETM+, and ALOS/AVNIR-2 satellite images used in this study.

Study sites	Corona date	Corona KH-4, KH-4A, and KH-4B	Landsat date	Landsat ETM+	ALOS date	ALOS/AVNIR-2
Darkhad depression	1962/08/29	DS009044048AF031 DS009044048AA036	1999/09/05	LE71370241999248	2006/09/17	AVNIR-2
Mungut river valley	1968/08/29	DS009044048AF024 DS009044048AA029	2000/09/07	LE71370262000251	2006/08/29	AVNIR-2
Chuluut river valley	1966/09/21	DS1035-1006DF075 DS1035-1006DA076	1999/08/22	LE71350271999234	2007/06/17	AVNIR-2
Khongor-Ulun	1968/08/11	DS1104-1055DF009 DS1104-1055DA015	2000/09/10	LE71420262000254	2007/09/01	AVNIR-2
Nalaikh depression	1968/08/16	DS1104-2135DF001 DS1104-2135DA005	1999/08/10	LE71310271999222	2007/06/07	AVNIR-2
Galuut depression	1964/06/10	DS1006-2085DF054 DS1104-2085DA058	1999/08/22	LE71350281999234	2007/09/27	AVNIR-2
Erdene	1962/08/29	DS009044032AF024 DS009044032AA030	2001/09/19	LE71360292001262	2006/08/31	AVNIR-2

4.2.1. Corona KH-4, KH-4A, and KH-4B satellite data

The high resolution images acquired from Corona camera systems KH-4, KH-4A, and KH-4B were declassified in 1995 and first became available in a digital format in 2003 (McDonald, 1995). The systems were equipped with both forward and backward looking cameras (Table 4.1). The satellite images have a higher spatial resolution (3.00-7.6 m, 2.70-7.6 m, and 1.8-7.6 m, respectively) at a scale between 1:247,500 and 1:305,000 and wide area coverage. They are available from the USGS Earth Resources Observation Systems (EROS) Data Center (Goossens *et al.*, 2006). The Corona images were scanned at 3600 dpi (7 microns) by USGS/EROS in a digital format. Of the total (15 × 290 km, 17 × 232 km and 14 × 188 km, respectively) ground coverage of Corona KH-4, KH-4A and KH-4B images.

On the other hand, Corona strips are known to contain significant geometric distortions (Altamaier *et al.*, 2002; Goossens *et al.*, 2006). Geometric distortion inherent in filmstrips from a panoramic camera need to be corrected achieve precise results (Slama, 1980). Typical geometric distortions of Corona image gradually increase from the center to the extreme edges of an image along the track (Figure 4.2).

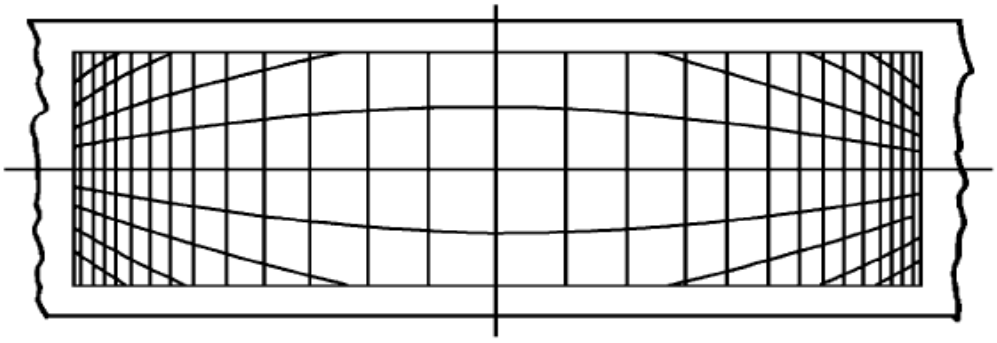

Figure 4.2. Geometric distortion of Corona satellite image (Slama, 1980).

Corona satellite images have been used for several years for different scientific purposes and in different regions of the world. It is especially useful in developing countries where aerial photographs in wide area coverage are rarely available. Beside the presented technical advantages, the high resolution Corona satellite images are also available at a reasonable price and provide an excellent opportunity for change detection studies.

Table 4.2. Important parameters of high-resolution satellite images used in this study.

Parameters	Corona KH-4	Corona KH-4A	Corona KH-4B	ALOS	Landsat
Time period	1962-1963	1963-1969	1967-1972	2006-2007	1999-2001
Camera/Sensor type	panoramic	panoramic	panoramic	AVNIR-2	ETM+
Focal length (cm)	60.96	60.96	60.96	790	
Ground resolution (m)	7.6	2.7	1.8	10	15 (band 8)
Flight altitude (km)	170 to 460	185	150	691	
Pixel scan (μm)	7 (3600dpi)	7 (3600dpi)	7 (3600dpi)		
Ground coverage (km)	15 x 290	17 x 232	14 x 188	70 x70	185x170

4.2.2. Landsat ETM+ satellite data

Landsat satellite imagery is available since 1972 from six satellites in the Landsat series. These satellites have been a major component of the National Aeronautics and Space Administration's (NASA) Earth observation program, with three primary sensors evolving over thirty years: MSS (Multi-spectral Scanner), TM (Thematic Mapper), and ETM+ (Enhanced Thematic Mapper Plus). Landsat supplies high resolution visible and infrared imagery, with thermal imagery and a panchromatic image also available from the ETM+ sensor. The observation bands of ETM+ are essentially the same seven bands as TM, and the newly added panchromatic band 8, with a high resolution of 15m was added.

Landsat ETM+ panchromatic images were obtained from the USGS Global Visualization Viewer with limited cloud coverage conditions. The Landsat ETM+ images have spatial resolutions of 30 m (multispectral) and 15 m (panchromatic) over an area of 180 × 180 km. In this study, a total seven Landsat ETM+ panchromatic images (band 8) from 1999 to 2001 were used (Table 4.1). All data sets were registered to Universal Transverse Mercator (UTM) coordinate system zones 46N, 47N and 48N, and elevation referenced to World Geodetic System (WGS) 1984 datum.

4.2.3. ALOS/AVNIR-2 satellite data

Advanced Land Observation Satellite (ALOS) has launched in 2006 from the Tanegashima Space Center. This satellite was one of the world's largest earth observation satellites whose function is to collect global and high resolution land observation data. The ALOS satellite sensor

had three remote-sensing instruments: the Panchromatic Remote-sensing Instrument for Stereo Mapping (PRISM) and for digital elevation models (DEM). The Advanced Visible and Near Infrared Radiometer type 2 (AVNIR-2) for precise land coverage observation, and the Phased Array type L-band Synthetic Aperture Radar (PALSAR) for day-and-night and all-weather land observation and enabled precise land coverage observation and can collect enough data by itself for mapping on a scale of 25,000:1, without relying on points of reference on the ground.

ALOS/AVNIR-2 satellite images between 2006 and 2007 (Table 4.1) were acquired from the Japan Aerospace Exploration Agency (JAXA). ALOS/AVNIR-2 is a satellite sensor that has four spectral bands and performance with a resolution of 10 m in the visible and near-infrared bands (ground coverage 70 × 70 km).

4.3. Remote sensing method

4.3.1. Orthorectification and image co-registrations

In this study, two major image processing tasks carried out were: orthorectification and image co-registration. Orthorectification is the process of making orthorectified images, which are in principle, map like distortion free corrected products. To geometrically correct and orthorectify the Corona strips, we used a non-metric camera model in ERDAS Leica Photogrammetric Suite (LPS) version 9.3 software at the PLANAR SD 2020 Stereo Mirror^{TM}/3D Monitor, where we assigned the focal length, the pixel size of the scanned scenes and flight altitude of the camera platform (Goossens *et al*., 2006).

The most of our study sites are mountain regions with high and medium relief. In such areas, some elevation data is essential to remove relief-induced displacement such as a kind of

geometric distortion; otherwise large distortion may occur. The Advanced Spaceborne Thermal Emission and Reflection (ASTER) Global Digital Elevation Model (GDEM) with 30 m spatial resolutions were used as the source of elevation data to orthorectify all datasets in this study. On the other hand, I also surveyed the ground control points at each study site and surrounding area during the field work on August to September 2009 which are needed to ortho-rectify of the high resolution satellite images. As stated earlier, ground control points (GCPs) for all data except the field data were collected from the Landsat ETM+ and ASTER GDEM in each site. We used the bundle block adjustment procedure in LPS to simultaneously estimate the orientation of all Corona strips based on ~100 ground control points (GCPs). Latitude (x) and longitude (y) information of the GCPs were extracted from the panchromatic Landsat ETM+ images (band 8), whereas elevation information (z) was extracted from the GDEM. All tie points were automatically placed at the correct locations on both images (forward and backward) in LPS. The Corona stripes were mosaicked in LPS to produce the final orthorectified images. Root mean square error (RMSE) of the aerial triangulation for Corona images were less than 15 m because of the small subset of data used at study sites.

Image co-registration is a process of mutually georefenrencing already orthorectified images based on a reference image for an accurate alignment of the dataset. These tasks were accomplished in order using remote sensing software as ERDAS IMAGINE. The ALOS/AVNIR-2 images were co-registered using the Landsat ETM+ images in AutoSync workstation of ERDAS based on at least 500 GCPs for each image. The orthorectified ALOS images were a maximum RMSE of less than 1 m. For consistency of data processing and presentation, all images were processed with different the projection parameters depends on

location of each study sites: categories-UTM WGS 84 North, projection-zones 46-48, spheroid-WGS 84, datum-WGS 84, and horizontal and vertical measurement unit-m.

4.3.2. Delineation and analyzing of thermokarst lakes

Firstly, we attempted the automated classification of lake areas based on the orthorectified images. However, we abandoned the automated spectral approaches commonly used in digital image processing due to the issues where cloud shadows creating dark patches that were spectrally similar to water, and sun glint near the edges of these images creating bright small lakes were confused bright target such as meadows (Grosse *et al*., 2005).

We visually delineated all lake areas from each satellite image at study sites that were above a minimum area of 0.1 ha (1000 m2). The shoreline of each lake was manually traced as a polygon area using ArcGIS 9.1 software (Figure 4.3). Finally, we categorized the extracted lake areas into four distinct classes (0.1 - 1 ha, 1 - 10 ha, 10 - 100 ha, and 100 - 1000 ha) in order to better understand the lake dynamics of individual lake size categories.

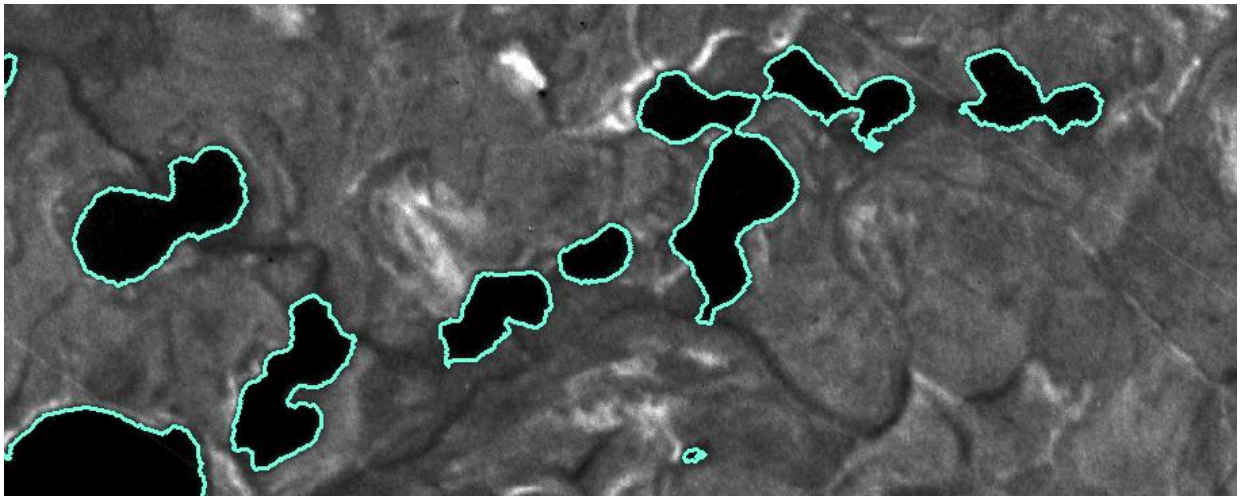

Figure 4.3. An example of the delineation for lake areas from Corona satellite image.

4.3.3. Lake water volume calculation

The water volume of lake and its vitiations over time are fundamental properties, reflect the balance between precipitation and evaporation (Brooks and Hayashi, 2002; Medina *et al*., 2010). The volume of water bodies at particular times can be calculated by several methods depending on the availability data. The volume of water in lakes is commonly estimated by combining data of water level variations with accurate bathymetry and shore topography maps (Lu *et al*., 2013). However, bathymetry and shore topography data are often difficult to acquire, due to high costs for labour and equipment. The development of satellite remote-sensing images over the last half century makes it possible to obtain information on the changes of water surface area of lakes at different times (Wu and Lu, 2010). It is easy to understand that a series of water surface boundaries of lake at different water levels are similar to contour lines on a digital elevation map and can be used to determine the boundaries elevation of that lake.

The main objective is to estimate the water volume of thermokarst lakes at the Darkhad and Galuut depressions. This study is used simple method for calculating of the water volume of lakes by using the extracted boundaries of lake areas in 1962/64, 1999, and 2006/07, ASTER GDEM, and mathematical equations relating area and volume to depth and water level (Figure 4.4). First, all lake water level (elevation) for each time period are determined by the extracted boundaries of lake areas and DEM data with 3D patch analysis at Global Mapper software. Finally, lake water volumes (between 1962/64 and 2006/07) were calculated by the basic mathematical equations. In addition, the appeared and disappeared lakes at two depressions were removed from this analysis.

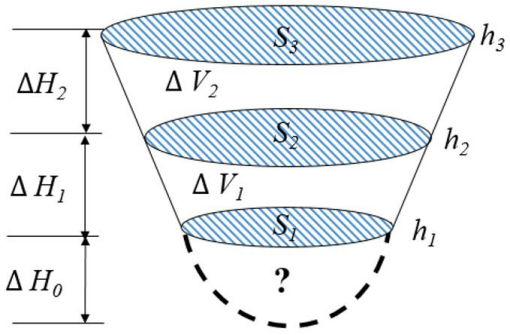

Figure 4.4. Calculating the water volume of layer of water in lake.

In this study, water volume is calculated as following equations (Taube, 2000):

$$\Delta H_1 = (h_1 - h_2) \quad \Delta H_2 = (h_2 - h_3) \qquad (1)$$

Where:

$\triangle H_{1,2}$ - difference in depth between two successive depth contours (m)

h_1, h_2, *and* h_3 - lake level in different time periods as 1962/64, 1999, and 2006/07 (m).

$$\Delta V_1 = \frac{1}{2}\Delta H_1 (S_1 + S_2)$$

$$\Delta V_2 = \frac{1}{2}\Delta H_2 (S_2 + S_3) \qquad (2)$$

Where:

$\triangle V_1$ – volume changes of the lake in 1962/64-1999 (m^3)

$\triangle V_2$ – volume changes of the lake in 1999-2006/07 (m^3)

$S_{1,2,3}$ – surface area of lake at depth h_1, h_2, *and* h_3 (m^2)

4.4. Results and Discussions

4.4.1. Thermokarst lake changes from 1962 to 2007

Figure 4.5 illustrates the mapping of thermokarst lake changes in the Darkhad depression in the continuous permafrost zone from 1962 to 2006, where is a predominance of small lakes. There were total 84 new lakes formed with a water surface area of 338 ha between 1962 and 2006, while the area of 173 lakes increased by 384 ha. However, some decreases in the lake areas were also observed. The surface area of four lakes did not change during the observation periods. Overall, the number of lakes increased from 296 to 371, and their area increased from 3350 ha to 3651 ha between 1962 and 2007, which are summarized in Table 4.3.

The behavior of these thermokarst lakes in the Darkhad depression can be explained by the several factors such as climate and permafrost changes. According to the climate change analysis, the water balance was showed negative value during last 45 years, which did not attribute with the expansion and formation of thermokarst lake. However, there are significant increasing trend resulted in the mean annual air temperature. This atmospheric warming probably leads to permafrost degradation. Cause, permafrost temperature has increased significantly in the site (Bat-Erdene, 1995, Jambaljav *et al*., 2013). Furthermore, the depression has an extensive flat floor underlain by thick lacustrine sediments (Ishikawa and Jambaljav, 2015) with deep ice-rich permafrost (Photo 1.1) and shallow active layers (Sharkhuu, 2011). These local permafrost conditions are more relative to thermokarst lake changes. Therefore, that the expansion and formation of lakes probably caused by the thaw of ice-rich permafrost. In continuous permafrost zone, Smith *et al*. (2005) reported the increasing number and area of thermokarst lakes in the western Siberia, and is similar with observations from this study site.

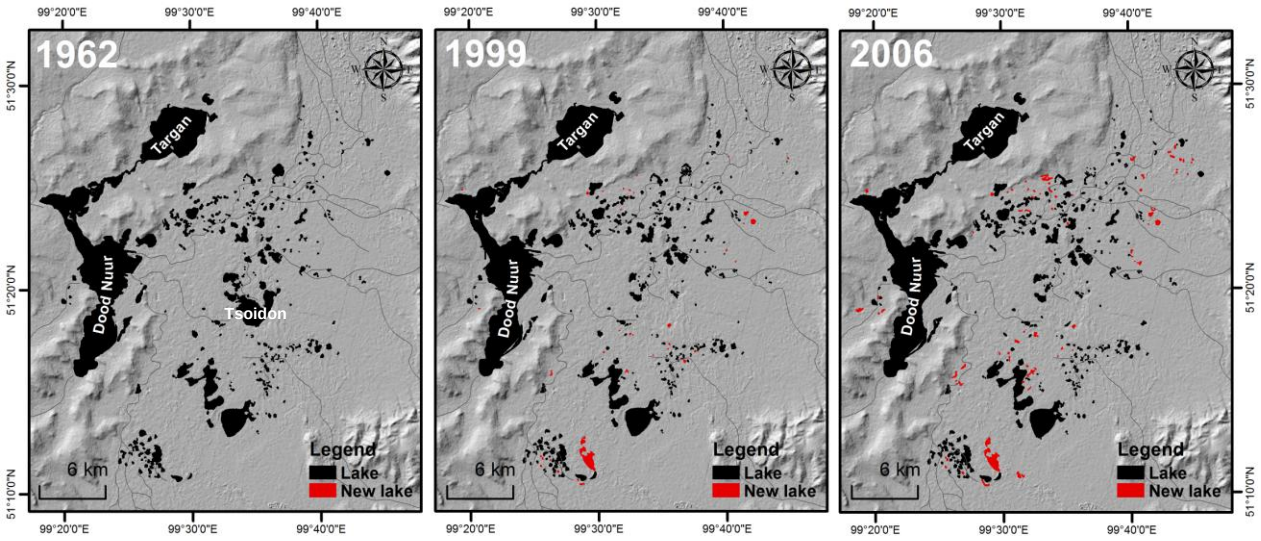

Figure 4.5. Mapping of thermokarst lake changes in the Darkhad depression from 1962 to 2006 in the continuous permafrost zone: very large lakes such as Dood Nuur, Targan, and Tsoidon are excluded from the recent analysis.

The number of lakes in the Mungut river valley remained stable throughout the whole study period (Table 4.3). However, area of lakes decreased from 161 ha to 122 ha between 1962 and 2007. Nevertheless, two lakes with a surface area of small sizes were formed, as illustrated in Figures 4.6. Thermokart lakes in the Chuluut river valley showed a decrease from 34 to 29 in number, and area (59 ha to 39 ha) respectively during the study period. Three small lakes appeared in this site (Figures 4.7). These results demonstrate the importance of analyzing both lake number and area to provide meaningful information for understanding thermokarst lake dynamics.

Permafrost temperatures have increased in these sites (Jambaljav *et al*., 2013). According to Sharkhuu (2011), thermokarst processes at the Chuluut river valley have started in late 1980s and leads to maximum subsidence in the late 1990s. For these valleys, ground ice contents characterized by medium and lacustrine sediments (Sharkhuu, 1969; Yoshikawa et al., 2013).

These combined facts at these sites may cause that formation of small lakes in the river valleys. As shown the results of climate changes, the negative water balances were observed at both sites, which might be attributed to the shrinking lake area and numbers.

Our results in lake number and area at both sites differ from Alaskan permafrost regions. Jones *et al*. (2011) identified thermokarst lake changes in Alaska. They found that lakes had increased in number, and decreased in area following partial drainage of large lakes.

Table 4.3. Thermokarst lake changes by sites and by permafrost zones over the study period.

Study sites	1962-1968		1999-2001		2006-2007	
	Number	Area (ha)	Number	Area (ha)	Number	Area (ha)
Darkhad depression	296	3350	350	3612	371	3651
Mungut river valley	7	161	7	141	7	122
Chuluut river valley	34	59	30	47	29	39
Khongor-Ulun	10	110	13	119	13	124
Nalaikh depression	2	7	1	5	1	1
Galuut depression	108	409	73	371	64	367
Erdene	8	6	3	4	3	3

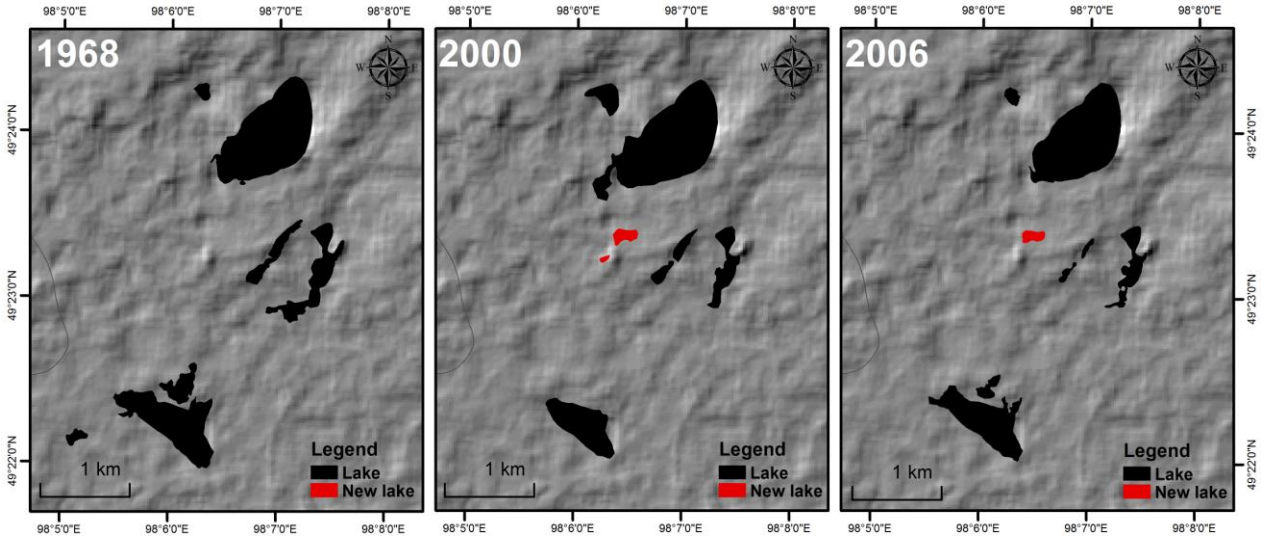

Figure 4.6. Mapping of thermokarst lake changes in the Mungut river valley from 1968 to 2006 in the continuous permafrost zone.

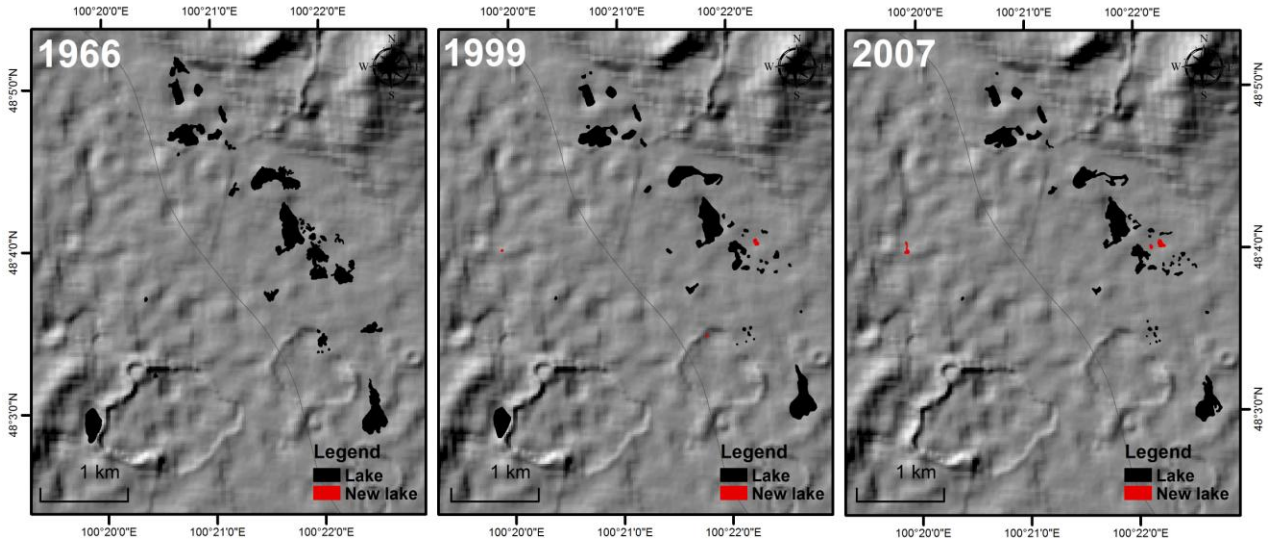

Figure 4.7. Mapping of thermokarst lake changes in the Chuluut river valley from 1966 to 2007 in the continuous permafrost zone.

In the Khongor-Ulun, ten lakes were delineated in 1962/68, then their number increased by 3 in 1999/01 and later remained stable for 2006/07 (Table 4.3). Seven lakes increased in size from 103 to 117 ha, and 3 new lakes appeared. Lake area in this site increased from 1962 to 2007 (Figure 4.8). These lake behaviors in the Khongor-Ulun are showed similar trends with Darkhad depression. However, ground ice-content has characterized low in the Khongor-Ulun. According to long-term borehole measurement, permafrost temperature is increased significantly due to the warming air temperature (Figure 3.4, and Figure 3.8). We did not found any significant changes in total annual precipitation. On the other hand, previous study reported (Tserensodnom, 2002), thermokarst lakes probably formed as a result of permafrost degradation, which are connected to channel outflow in this site, they did not determine their changes of area and number. These information can be supported to the expansion and formation of thermokarst lakes.

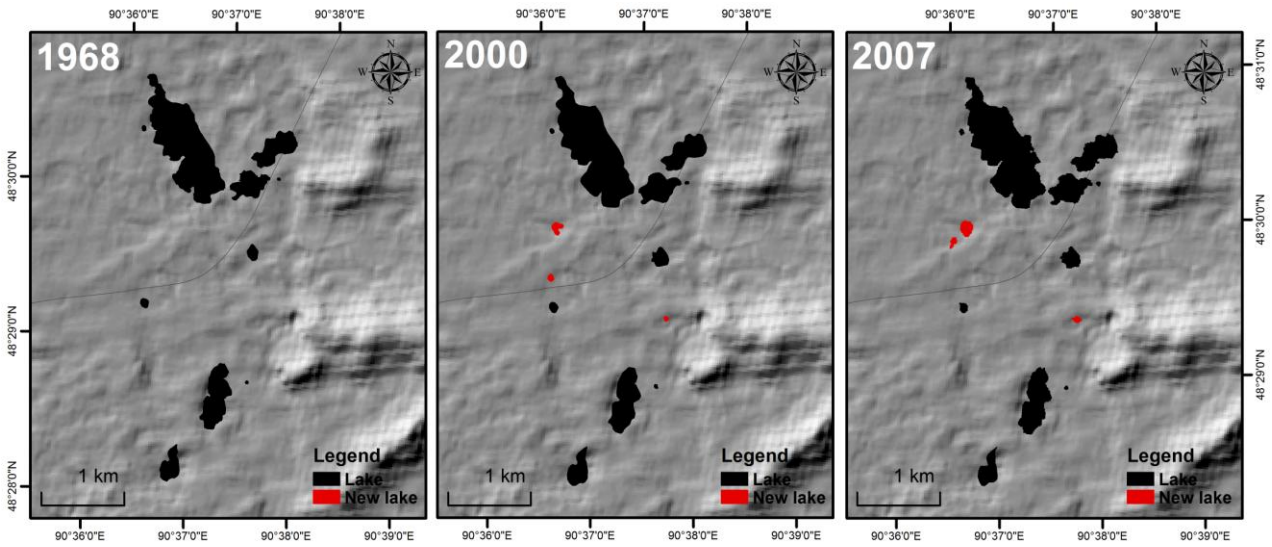

Figure 4.8. Mapping of thermokarst lake changes in the Khongor-Ulun from 1968 to 2007 in the continuous permafrost zone.

For the continuous permafrost zone, the total number of lakes increased by 73, from 347 in 1962/68 to 420 in 2006/07 (Table 4.3). The total lake area shows similar pattern as the lake number, increasing the total area of lakes over the study period (1962/68 to 2006/07) from 3680 ha to 3936 ha.

On the other hand, for the isolated permafrost zone, only two lakes were determined in the Nalaikh depression (1968), and one of them drained before 1999/01 (Figure 4.9, and Table 4.3). In terms of lake area change, there was a decrease of 6 ha for this site. While, the observed lakes in Galuut depression decreased both in number and area from 1962 to 2007, respectively. Many small lakes were disappeared in this area (Figure 4.10). In the Erdene, lake number shows a decrease of 5 between 1962/68 and 1999/01, but remained stable afterwards for 2006/07 (Figure 4.9, and Table 4.3). However, lake area decreased by 3 ha in 2006/07. In the isolated permafrost zone, the investigated thermokarst lakes have greatly decreased in number and area between 1962 and 2007 as result of lake drainage. Overall, a total of 118 lakes (422 ha) were delineated in the isolated permafrost zone for the period of 1962/68. The number of lakes decreased by 50 lakes in 2007. The total area of lakes decreased by 51 ha during the last 45 years.

The above mentioned results in the Nalaikh depression, Galuut depression, and Erdene are could be explained by long-term climate and permafrost changes. The observed reduction in number and area of lakes in the southern isolated permafrost zone may be due to a combination of several factors including the air temperature, the potential evapotranspiration, and negative water balance, as well as permafrost disappearance (Sharkhuu *et al*., 2008 and 2011; Ishikawa *et al*., 2012; Jambaljav *et al*., 2013). The mean annual air temperature trends increased slightly in these sites in the isolated permafrost zone from 1962 to 2007 (Table 3.1). Furthermore, a

decreasing trend of mean annual air temperature and a positive water balance were found in the Erdene, such results were not consisted with the lake reduction. From our analysis, we found no significant correlation between the total annual evapotranspiration and reduction of lakes in these sites. Thus, lakes might have correlated with the subsurface drainage and deepening active layers in the isolated permafrost zone.

Shrinking and disappearing thermokarst lakes may become a common feature in the discontinuous, sporadic and isolated permafrost zones as a consequence of warming climate and disappearing permafrost (Yoshikawa and Hinzman, 2003). Our results were consistent with lake reductions observed by other similar studies (Yoshikawa and Hinzman, 2003; Smith *et al*., 2005; Riordan *et al*, 2006). Smith *et al*. (2005) used satellite imagery from 1970s to 2004 to document the decline of thousand lakes in Siberia. Their study showed an increase of total lake number and area in the continuous permafrost zone, and a contrasting decrease in discontinuous to isolated permafrost zone. We also found a substantial reduction in the total number and area of thermokarst lakes in the isolated permafrost zone in Mongolia.

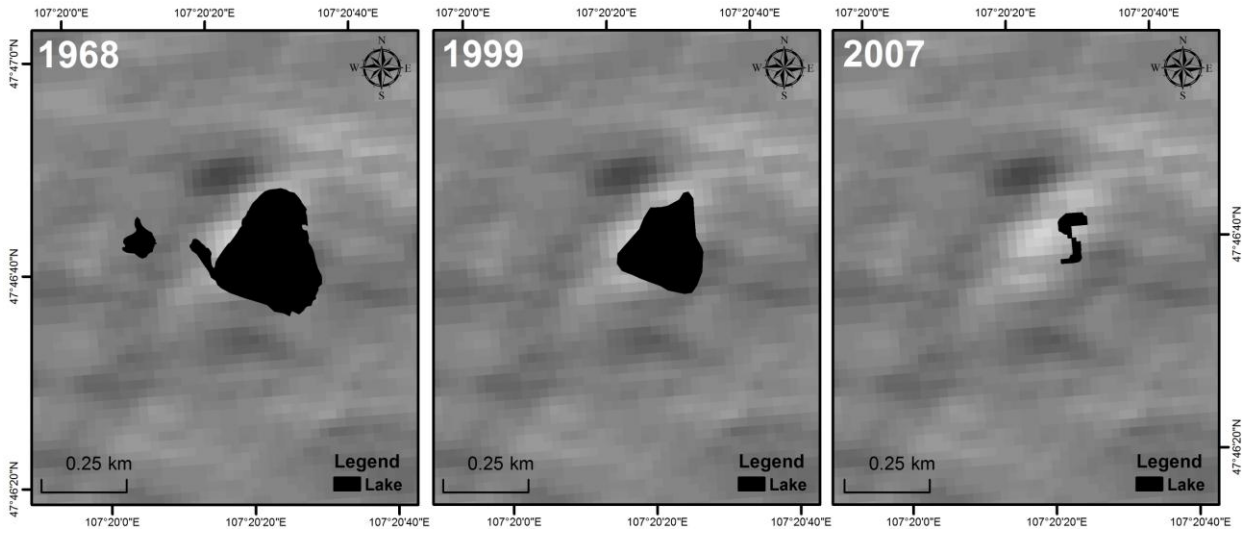

Figure 4.9. Mapping of thermokarst lake changes in the Nalaikh depression from 1968 to 2007 in the isolated permafrost zone.

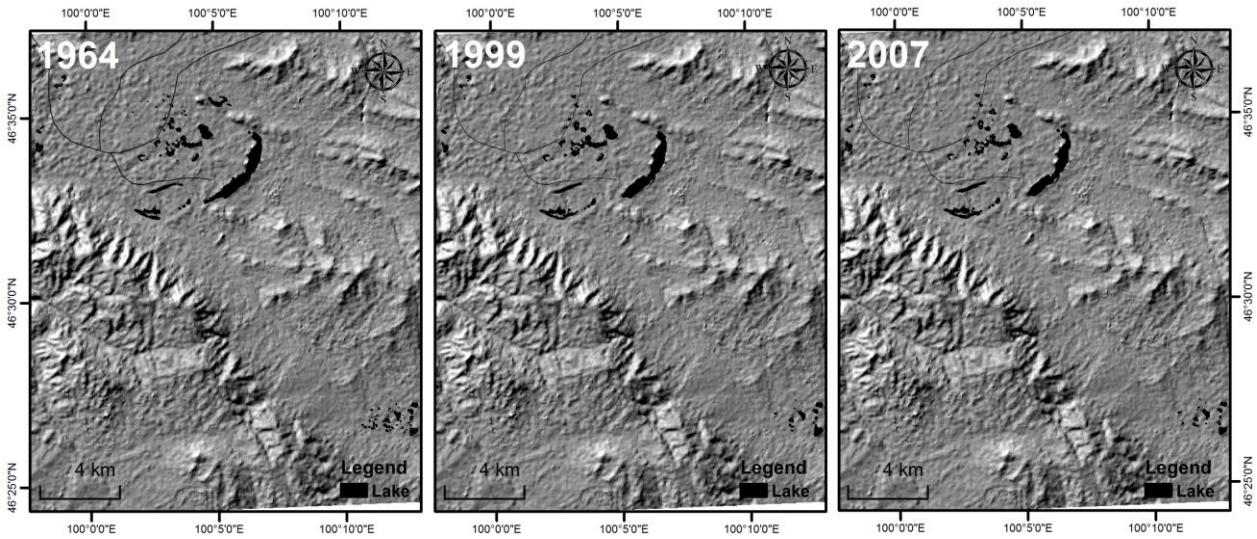

Figure 4.10. Mapping of thermokarst lake changes in the Galuut depression from 1964 to 2007 in the isolated permafrost zone.

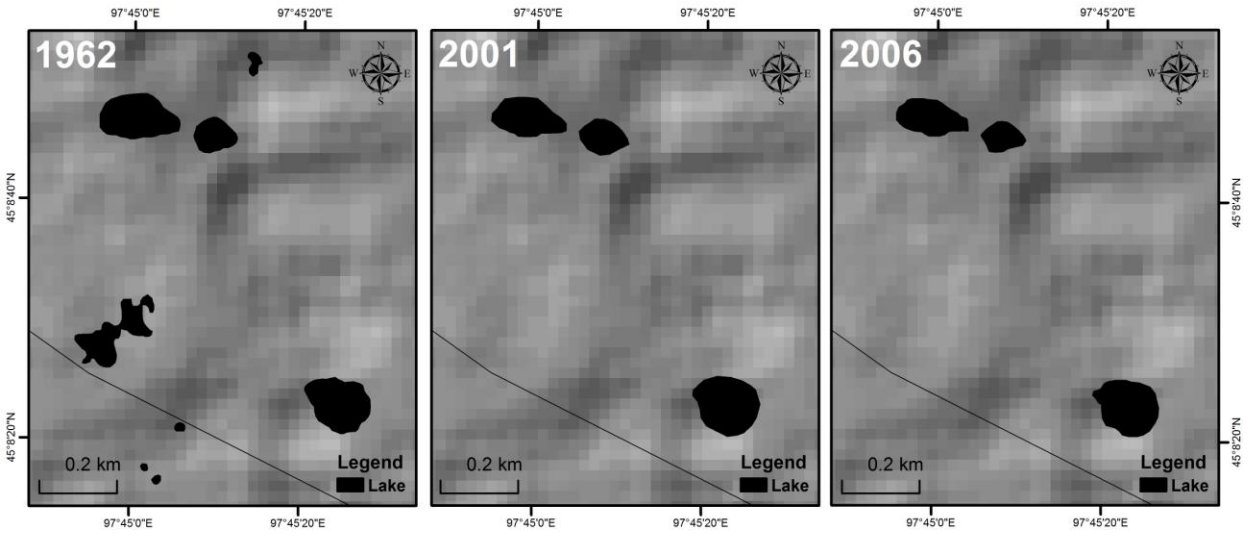

Figure 4.11. Mapping of thermokarst lake changes in the Erdene from 1962 to 2006 in the isolated permafrost zone.

4.4.2. Frequency of the number and area of thermokarst lakes

We identified total 1430 lakes on the continuous and isolated permafrost zones. The total changes of thermokarst lakes subdivided by lake area size are illustrated in Figure 4.12. We further summarized the results of lake changes in the continuous permafrost zone (Darkhad depression, Mungut river valley, Chuluut river valley, and Khongor-Ulun), and isolated permafrost zone (Nalaikh depression, Galuut depression, and Erdene).

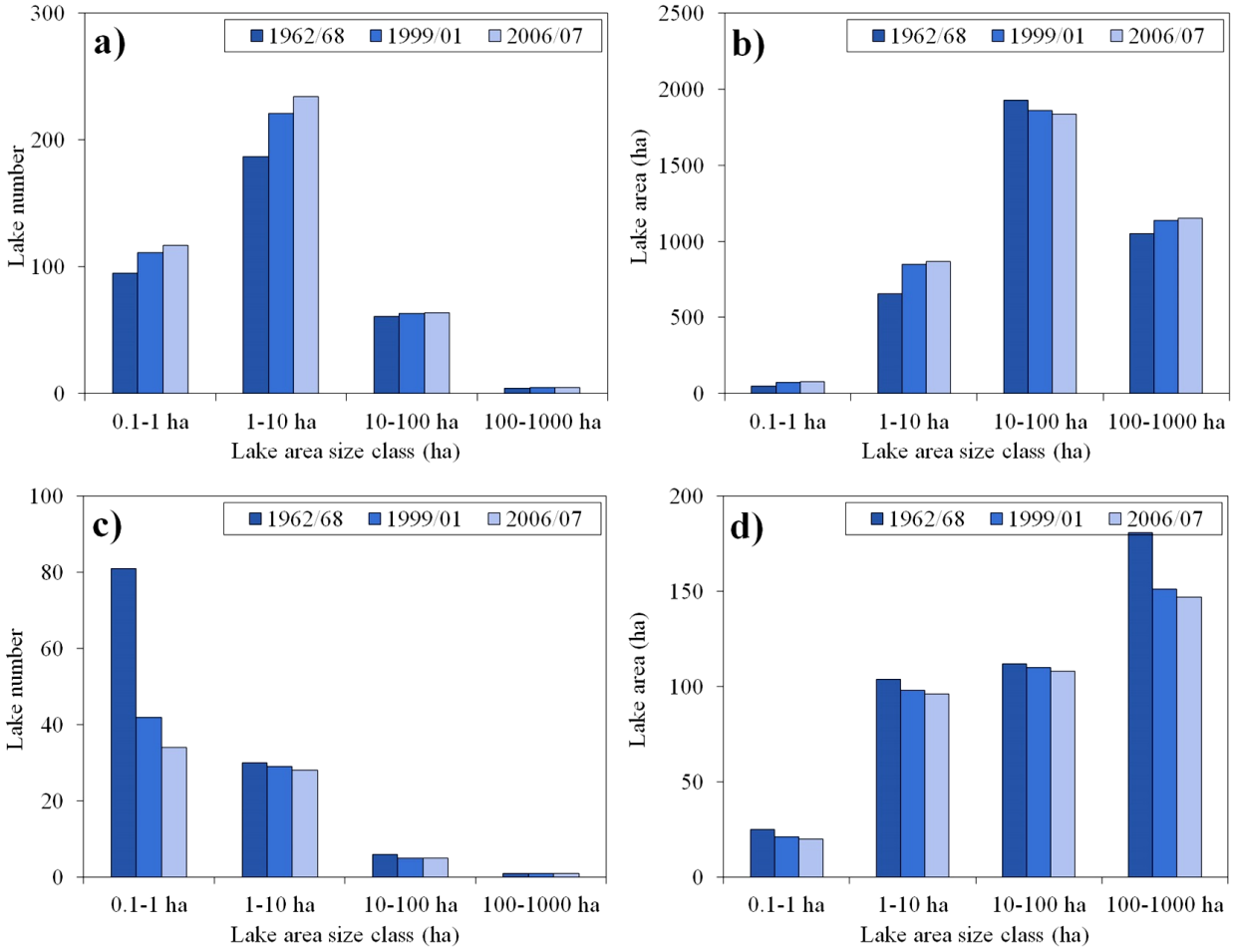

Figure 4.12. Lake size classes in the continuous (a-number; b-area of lakes), and isolated (c-number; d-area of lakes) permafrost zones for 1962-2007.

The number and area of lakes in size class 0.1 - 1 ha greatly increased from 95 (48 ha) in 1962/68, to 111 (73 ha) in 1999/01, to 117 (77 ha) in 2006/07 in the continuous permafrost zone (Figure 4.12-a, and b). The next smallest size class of 1-10 ha also experienced a large change in both lake number (+47) and area (+215 ha) from 1962 to 2007. The number of lakes (10 - 100 ha) increased slightly (+3) from 1962 to 2007, however, their area decreased by 91 ha during the same time period. The large size class 100 - 1000 ha also expanded by 103 ha in the area of lakes since 1962, and the lake number actually increased in 1999/01 and remained stable in 2006/07.

The increases in both number and area of lakes can be explained by the formation of new lakes as results of permafrost thaw due to climate warming. Figure 4.13 shows one example for the formation of new thermokarst lake based on visual inspection.

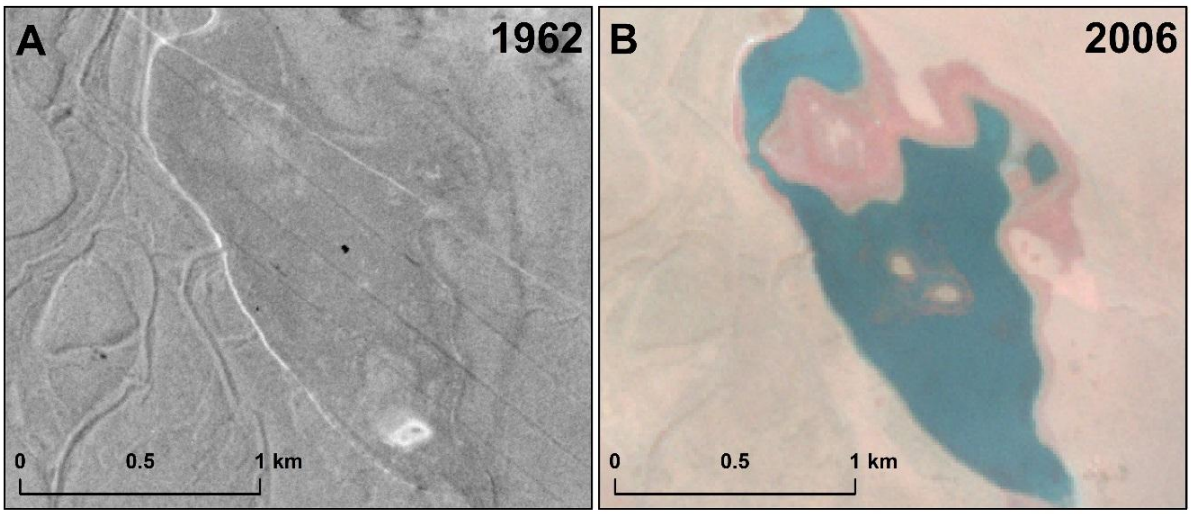

Figure 4.13. An example for the formation of new thermokarst lake in the Darkhad depression, the continuous permafrost zone from 1962 (a – Corona satellite image) to 2006 (b – ALOS satellite image).

In the isolated permafrost zone, there is a predominance of smaller lakes as shown in (Figure 4.12-c, and d), which divides thermokarst lakes into four size classes. From 1962 to 2007, the number of lakes decreased in all size classes (except 100 - 1000 ha), and the most reduction (from 117 lakes to 67 lakes) occurred in lake size classes between 0.1 - 1 ha and 10 - 100 ha. Large lake size class of 100-1000 ha was 181 ha (1962/68) and decreased by 34 ha (2006/07). Between 1962 and 2007, lake area decreased in all lake classes. In fact, fifty lakes completely disappeared in the Nalaikh depression, Galuut depression, and Erdene. Most of the disappeared lakes had an area of less than 1 ha. Figure 4.14 illustrates the disappeared thermokarst lake in the Galuut depression between 1964 and 2007.

These results highlight the importance of the high resolution images, which can reveal complex spatiotemporal changes to better understand of lake dynamics of individual lake size categories

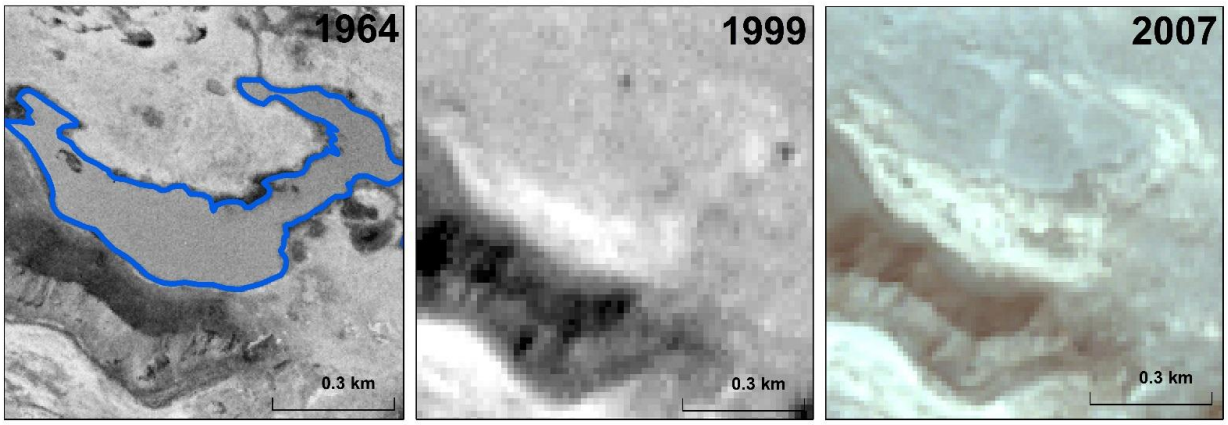

Figure 4.14. An example of thermokarst lake that has been drained in the Galuut depression, the isolated permafrost zone from 1964 to 2007. Blue polygon represents the water surface area of lake.

4.4.3. Volume changes of thermokarst lakes (1962-2007)

This study is calculated volume changes of thermokarst lakes in Darkhad and Galuut depressions, which are located in the continuous and isolated permafrost zones, respectively. Most of thermokarst lakes in the study were demonstrated for these depressions. Their topography were quite different on the floor (Figure 4.15). As shown the map, Darkhad depression has characterized by the highly undulated terrain (Figure 4.15-a), in contrast, it is gently undulated landscapes in Galuut depression (Figure 4.15-b). These differences on topography and permafrost conditions would be interesting for volume changes of thermokarst lakes.

Figure 4.16 shows the volume changes of thermokarst lakes in the continuous and isolated permafrost zones. The estimated volume changes of thermokarst lakes in the Darkhad depression are increased largely for lake sizes (1-10 ha to 100-1000 ha) between 1962 and 2007 (Figure 4.16-a), however, they increased slightly in small lake (0.1-1 ha). This result is likely attributed to the increasing area and number of lakes in the depression (Table 4.3). Number of small lakes was increased rapidly during the observation period (Figure 4.12), which may be linked to the undulated terrain. The area and volume changes of thermokarst lakes probably initiated as ice-rich permafrost thaws.

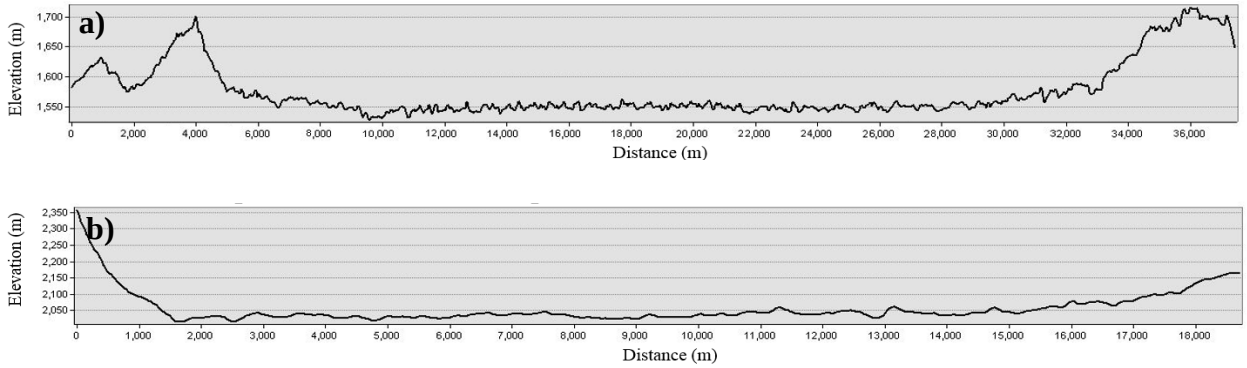

Figure 4.15. Topographic maps of (a) Darkhad depression in the continuous permafrost zone, and (b) Galuut depression in the isolated permafrost zone. Map produced by ASTER GDEM.

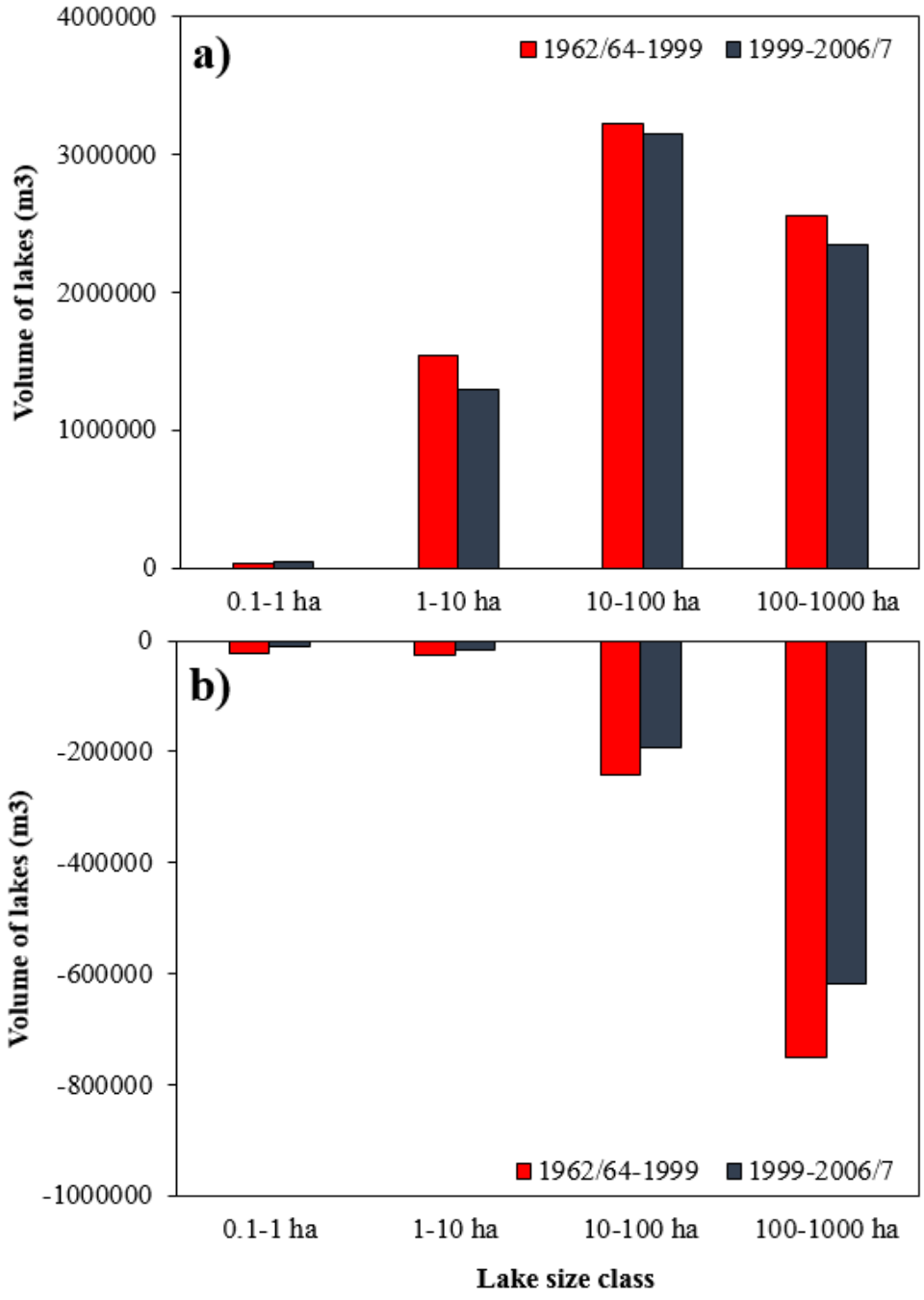

Figure 4.16. Volume changes of thermokarst lakes: (a) Darkhad depression in the continuous permafrost zone, and (b) Galuut depression in the isolated permafrost zone.

In the isolated permafrost zone, volume changes of thermokarst lakes showed a decreasing trends for all lake sizes during the last 45 years, especially lake sizes larger than 10 ha (Figure 4.15-b). This would be consistent with the above mentioned results on number and area of lakes in the depression. During the observation period, lakes were disappeared and decreased in the area (Table 4.3), which directly influenced for volume changes of these lakes. One possible reason for the decreasing volume changes of lakes may be linked to smooth topography or subsurface drainage of permafrost.

4.5. Conclusion

The main conclusions of this chapter are as follows:

1. This study demonstrated that high-resolution Corona, Landsat ETM+, and ALOS/AVNIR-2 satellite imagery are more useful for precise delineation of thermokarst lakes area.

2. In the continuous permafrost zone, total surface area and number of thermokarst lakes increased by +21% (347 to 420), and +7% (3680ha to 3936 ha), respectively. In contrary, their decreased by -40% (118 to 68) in number, and -10% (422 ha to 371 ha) in area. These results likely attributed with the appearing and disappearing lakes.

3. We found significant differences in the spatio-temporal dynamics of thermokarst lakes in the continuous and isolated permafrost zones. This difference concerns the lake size classification. The number and area of small lakes between 0.1 and 10 ha increased more dramatically than large lakes in the continuous permafrost zone. In the isolated permafrost zone, however, small lakes (0.1 - 1 ha) had a significant reduction in number in the isolated permafrost zone.

4. The volume changes of thermokarst lakes are increased in the continuous permafrost zones (Darkhad depression), which is likely attributed to the increasing area and number of lakes in the depression. In the isolated permafrost zone, in contrast, that the volume changes observed only negative values (Galuut depression).

Chapter V. General discussion

This study identified the total 1430 thermokarst lakes in the continuous and isolated permafrost zones during the last 45 years. Contrasting changes in thermokarst lake dynamics were observed at seven study sites in Mongolia. That the results showed spatially heterogeneous patterns in lake changes with identified increasing and decreasing lake number and areas for the continuous permafrost sites. The increase in both number and area of lakes in the Darkhad depression and Khongor-Ulun can be explained by the formation of new lakes as results of permafrost thaw due to ongoing atmospheric warming. While many new lakes were found in the Darkhad depression, where total of 53 lakes appeared in 142 ha in 1999/01 and 32 lakes appeared in 24 ha in 2006/07, only a few lakes appeared in Khongor-Ulun. Decrease in Mungut river valley and Chuluut river valley is a result of large lakes become fragmented following partial drainage. These results demonstrate the importance of analyzing both lake number and area to provide meaningful information for understanding thermokarst lake dynamics. The overall growth in the area of lakes was due mostly to the expansion and appearance of lakes. Total numbers of lakes have increased by 85 in the continuous permafrost zone. This is demonstrated by the appearance of small lakes with areas of less than 10 ha. An increase in the number of lakes was reported in the west Siberian continuous permafrost zone (Smith *et al.*, 2005). In this study, we found a similar trend in the continuous permafrost zone in Mongolia. However, in the isolated permafrost zone, lake area and the number of lakes are decreasing, which is similar to the trend observed in other regions (Yoshikawa and Hinzman, 2003; Smith *et al.*, 2005; Riordan *et al.*, 2006).

We attribute the increase in area and number of lakes observed in the continuous permafrost zone to ongoing warming (Figures 3.6 and 3.8), which has been found as the main

driver for thermokarst lake expansion in this permafrost zone (Smith *et al*., 2005; Jorgenson *et al*., 2006). During the last 45 years, MAAT and PET increased significantly at the Darkhad depression, Mungut and Chuluut river valleys, and Khongor-Ulun in the northern continuous permafrost zone which are correlated with horizontal distribution of MAAT pattern. Such persistent warming trend has enhanced the permafrost degradation in northern Mongolia (Davaa and Jambaljav, 2014). As a result, new thermokarst lakes were probably formed in the continuous permafrost zone (Figure 4.12 and 4.13) may due to ice-rich permafrost thaw and ground surface subsidence.

On the other hand, the observed reduction in number and area of lakes in the southern isolated permafrost zone may be due to a combination of several factors including the air temperature, the potential evapotranspiration, and negative water balance, as well as permafrost disappearance (Davaa and Jambaljav, 2014). The MAAT trend increased slightly at Nalaikh depression and Galuut depression in the isolated permafrost zone from 1962 to 2007. Furthermore, a decreasing trend of MAAT with an increasing P was found at Erdene, such results were not consisted with the lake reduction. From our analysis, we found no significant correlation between the total annual PET and reduction of lakes in these sites. However, the total annual PET was higher at Nalaikh depression, Galuut depression, and Erdene in the isolated permafrost zone than Darkhad depression, Mungut river valley, Chuluut river valley, and Khongor-Ulun in the continuous permafrost zone. Potentially, the reduction in area and number of thermokarst lakes, especially small lakes, it likely associated with negative water balance (P-PET), the disappearing permafrost and subsurface drainage observed in the isolated permafrost zone (Yoshikawa and Hinzman, 2003; Riordan *et al.*, 2006).

Chapter VI. General conclusion

This thesis quantified spatiotemporal changes of thermokarst lakes dynamics at seven sites in the continuous and isolated permafrost zones of Mongolia from 1962 to 2007 using high-resolution Corona KH-4, KH-4A, and KH-4B, Landsat ETM+ (panchromatic), and ALOS/AVNIR-2 satellite imagery. The following conclusions are demonstrated from this study.

1. We found contrasting changes of thermokarst lake dynamics in the continuous and isolated permafrost zones. Thermokarst lakes in the continuous permafrost zone have increased significantly in number and area during the last 45 years. However, they decreased both number and area in the isolated permafrost.
2. The dramatic increase in number of smaller lakes with sizes between 0.1 - 1 ha and 1 - 10 ha compared to larger lakes (10 - 100 ha and 100-1000 ha) in the continuous permafrost zone is likely as a result of permafrost degradation due to increasing temperature and evaporations. However, small lakes (0.1 - 1 ha) had a significant reduction in number in the isolated permafrost zone. The reduction of thermokarst lake number and area might have attribute to a combination of disappearing permafrost, deepening of the active layer and an increase water loss in this permafrost zone.
3. The changes of thermokarst lakes in Mongolia are likely attributed to shifts in climate regimes and local permafrost conditions. Since 1962, the mean annual air temperature and potential evapotranspiration have increased significantly in the northern continuous permafrost zone compared to the southern isolated permafrost zone. Due to ongoing atmospheric warming without any significant trend in annual

precipitation, patches of ice-rich subsurface have thawed, and the number and area of lakes have accordingly developed in the continuous permafrost zone. Shrinking of thermokarst lakes in the isolated permafrost zone may be due to disappearing permafrost, deepening of the active layer, and increased water loss through surface evaporation and subsurface drainage.

4. The volume changes of thermokarst lakes are increased in the continuous permafrost zones (Darkhad depression), which is likely attributed to the increasing area and number of lakes in the depression. In the isolated permafrost zone, in contrast, that the volume changes observed only negative values (Galuut depression).
5. The time series data of high-resolution satellite imagery demonstrated useful in determining changes in the number and areal extent of thermokarst lakes greater than 0.1 ha in Mongolia from 1962 to 2007.
6. This study provides the first baseline information of thermokarst lake changes across Mongolia, filling the gap in sub-Arctic lake inventories at regional scales such as the southern fringe of Siberian permafrost region.

References

Anderson L, Birks J, Rover J, Guldager N. 2013. Control on recent Alaskan lake changes identified from water isotopes and remote sensing, Journal of Geophysical Research Letter, 40: 3413-3418.

Andresen CG, Lougheed VL. 2014. Disappearing Arctic Tundra Ponds: Fine-Scale Analysis of Surface Hydrology in Drained Thaw Lake Basins over a 65 Year Period (1948-2013). Journal of Geophysical Research, Biogeosciences, 120, 466-479. http://onlinelibrary.wiley.com/doi/10.1002/2014JG002778/epdf

Altamaier A, Kany Ch. 2002. Digital surface model generation from CORONA satellite images. Photogrammetry and Remote Sensing 56: 221-235.

Assessments of Impacts and Adaptations to Climate Change (AIACC), 2005.

Bat-Erdene D. 1995. Heat flow of rocks in the territory of Mongolia and its impact on the permafrost. Questions of Geography of Mongolia 30: 45-60 (in Mongolia).

Biskaborn BK, Herzschuh U, Bolshiyanov DY, Schwamborn G, Diekmann B. 2013. Thermokarst processes and depositional events in a Tundra lake, northeastern Siberia. Permafrost and Periglacial Processes 24: 160-174. DOI: 10.1002/ppp.1769.

Brooks RT, Hayashi M. 2002. Depth-Area-Volume and Hydroperiod Relationships of Ephemeral (Vernal) Forest Pools in Southern New England. Wetlands 22: 247–255.

Brown RJE, PeweTL. 1973. Distribution of permafrost in North America and its relationship to the environmental: a review, 1963-1973; in Proceedings Second International Conference

on Permafrost, North American Contribution, National Academy of Sciences, Washington, D.C., p 71-100.

Brown J, Ferrians OJ, Heginbottom JA, Melnikov ES. 1997. Circum-Arctic map of permafrost and ground-ice conditions. Circum-Pacific Map Series CP-45, scale 1:10,000,000, 1 sheet. US Geological Survey in Cooperation with the Circum-Pacific Council for Energy and Mineral Resources.

Dagvador D, Khuldorj B, Aldover RZ. 2009. In: Mongolia Assessment Report on Climate Change 2009. First Edition. Ulaanbaatar, Mongolia. Vol. 1: 1-228.

Davaa G, Jambaljav Ya. 2014. Water resources, glacier and permafrost. In: Mongolia-Second Assessment Report on Climate Change, Second Edition. Davagdorj D, Batjargal Z, Natsagdorj L (eds). Ulaanbaatar: Mongolia; Vol. 2: 109-127.

Dorjsuren Ch. 2014. Forest ecosystem. In: Mongolia-Second Assessment Report on Climate Change, Second Edition. Dagvadorj D, Batjargal Z, Natsagdorj L (eds). Ulaanbaatar: Mongolia; Vol. 2: 94-100.

Dashora A, Lohani B, Malik JN. 2007. A Repository of Earth Resource Information-CORONA satellite program. Current Science, 92, 926–932. http://home.iitk.ac.in/~javed/malik%20sir%20papers/10-Dashora-etal-Curr-Sci-2007.pdf

Frohn R C, Hinkel KM, Eisner WR. 2005. Satellite remote sensing classification of thaw lakes and drained thaw lake basins on the North Slope of Alaska, Remote Sensing Environment, 97, 116–126.

Goossens R, Wulf AD, Bourgeois J, Cheyle W, Willems T. 2006. Satellite imagery and archaeology: the example of Corona in the Altai Mountains. Journal of Archaeological

Science 33: 745-755.

Grosse G, Schirrmeister L, Kunitsky VV, Hubberten HW. (2005) The Use of CORONA Images in Remote Sensing of Periglacial Geomorphology: An Illustration from the NE-Siberian Coast. Permafrost and Periglacial Processes, 16, 163-172. http://onlinelibrary.wiley.com/doi/10.1002/ppp.509/pdf

Grosse G, Jones B, Arp C. 2013. Thermokarst lakes, drainage, and drained basins. In: John Shroder F (Editor-in chief), Giardino R, Harbor J (Volume Editors). Treatise on Geomorphology, Vol 8, Glacial and Periglacial Geomorphology, San Diego: Academic Press; 325-353.

Hinkel KM, Jones MB, Eisner RW, Cuomo JC, Beck AR, Frohn R. 2007. Methods to assess natural and anthropogenic thaw lake drainage on the western Arctic coastal plain of northern Alaska. Journal of Geophysical Research 112: F02S16.

Hinkel KM, Lenters JD, Sheng Y, Lyons EA, Beck EA, Eisner WR, Maurer EF, Wang J, and Potter BL. 2012. Thermokarst lakes on the Arctic coastal plain of Alaska: spatial and temporal variability in summer water temperature. Permafrost and Periglacial Processes 23: 207-217.

Hinzman, L.D., Goring, D.J. and Kane, D.L. 1998. A Distributed Thermal Model for Calculating Soil Thermal Temperature Profiles and Depth of Thaw in Permafrost Regions. Journal of Geophysical Research, 103, 975-991.

Intergovernmental Panel on Climate Change (IPCC). 2013.

Ishikawa M, Zhang Y, Kadota T, Ohata T. 2006. Hydrothermal regimes of the dry active layer. Water Resource Research 42:W04401. DOI:10.1029/2005WR004200.

Ishikawa M, Sharkhuu N, Jambaljav Ya, Davaa G, Yoshikawa K, Ohata T. 2012. Thermal state of Mongolian permafrost. In: Proceedings of the Tenth International Conference on Permafrost. Vol 1. 25-29 June, 2012, Hinkel KM (ed). Salekhard, Russia; 173-178.

Ishikawa M, Jambaljav Ya. 2015. Formation Chronology of Arsain Pingo, Darhad Basin, Northern Mongolia. Permafrost and Periglacial Processes, 27, 297-306.

Jambaljav Ya, Vanchig T, Battogtokh D, Saruulzaya A, Gansukh Ya, Temuujin Kh, Amarbaysgalan Yo. 2013. Scientific Report of Long Term Monitoring on Mongolian permafrost region. Dorjgotov D, Ed. Institute of Geography, Mongolian Academy of Sciences, Ulaanbaatar, Mongolia, 1-321.

JAXA (Japan Aerospace Exploration Agency). 2009.

Jones BM, Grosse G, Arp CD, Jones MC, Walter Anthony KM, Romanovsky VE. 2011. Modern thermokarst lake dynamics in the continuous permafrost zone, northern Seward Peninsula, Alaska. Journal of Geophysical Research 116:G00M03.

Jorgenson MT, Shur YL, Pullman ER. 2006. Abrupt increase in permafrost degradation in Arctic Alaska. Geophysical Research Letter 33: 4 (L02503).

Kanlay L. 1996. The NCEP/NCAR 40-year reanalysis project. Bulletin of the American Meteorological Society 77: 437-470.

Karlsson JM, Lyon SW, Destouni G. 2014. Temporal behavior of lake size-distribution in a thawing permafrost landscape in northwestern Siberia. Remote Sensing 6:621-636; doi:10.3390/rs6010621.

Krivonogova SK, Vladimir S, Sheinkmanb T, Anatoly A, Mistruykova B. 2005. Stages in the development of the Darhad dammed lake (Northern Mongolia) during the Late Pleistocene and Holocene, Quaternary International 136: 83–94.

Krivonogov SK, Yi S, Kashiwaya K, Kim JC, Narantsetseg T, Oyunchimeg T, Safonova IY, Kazansky AY, Sitnikova T, Kim JY, Hasebe N. 2012. Solved and unsolved problems of sedimentation, glaciation and paleolakes of the Dakhad Basin, northern Mongolia. Quaternary Science Reviews 56: 142-163.

Labrecque S, Lacelle D, Duguay C, Lauriol B, Hawkings J. 2009. Contemporary (1951-2001) evolution of lakes in the Old Crow Basin, northern Yukon, Canada, Remote sensing, numerical modeling, and stable isotope analysis. Arctic 62: 225-238.

Ling F, Wu Q, Zhang T, Niu F. 2012. Modelling open-talik formation and permafrost lateral thaw under a thermokarst lake, Beiluhe, Qinghai-Tibet Plateau. Permafrost and Periglacial Processes 23: 312–321.

Lu Sh, Ouyang N, Wu B, Wei Y, Tesemma Z. 2013. Lake water volume calculation with time series remote-sensing images. International Journal of Remote Sensing. Vol. 34, No.22, 7962-7973.

Manasypov RM, Pokrovsky OS, Kirpotin SN, Shirokova LS. 2014. Thermokarst lake waters across the permafrost zones of western Siberia. The Cryosphere 8:1177-1193.

Marsh P, Russell M, Pohl S, Haywood H, Onclin C. 2009. Changes in thaw lake drainage in the western Canadain Arctic from 1950 to 2000. Hydrological Processes 23: 145-158.

Medina CE, Gomez-Enri J, Alonso JJ, Villares P. 2010. Water Volume Variations in Lake Izabal from In Situ Measurements and ENVISAT Radar Altimeter and Advanced Synthetic Aperture Radar Data Products. Journal of Hydrology 382: 34–48.

Mongolia Assessment Report on Climate Change (MARCC). 2009. First Edition. Ulaanbaatar, Mongolia. Vol. 1: 1-228.

Mongolia Assessment Report on Climate Change (MARCC). 2014. Second Edition. Ulaanbaatar, Mongolia. Vol. 2: 1-302.

McCabe GJ, Markstrom SL. 2007. A Monthly Water-Balance Model Driven by a Graphical User Interface.

McDonald RA. 1995. CORONA: Success for space reconnaissance, a look into the Cold War, and a revolution for intelligence, Photogrammetric Engineering & Remote Sensing, 61(6):689–720.

Morgenstern A, Grosse G, Gunther F, Fedorova I, Schirrmeister L. 2011. Spatial analysis of thermokarst lakes and basins in Yedoma landscapes of the Lena Delta. The Cryosphere 5: 849-867.

Melnikov PI. (Ed.). 1974. Geocryological Conditions of Public Republic Mongolia. Proceedings of Joint Soviet-Mongolian Research Geological Expedition, vol. 10. Nauka, Moscow.

Natsagdorj L, Sarantuya G. 2014. Climate research and observed climate change in Mongolia. In: Mongolia-Second Assessment Report on Climate Change, Second Edition. Dagvadorj D, Batjargal Z, Natsagdorj L (eds). Ulaanbaatar: Mongolia; Vol. 2: 59-69.

Nishida H, Jamsran Ts (eds.). 2009. Darkhadyn wetland in Mongolia: synthesis investigation on ecosystems. NPO Mongolia Ecology Information Center, Japan.

Niu F, Lin Zh, Liu H, Li J. 2011. Characteristics of thermokarst lakes and their influence on permafrost in Qinghai-Tibet Plateau. Geomorphology 132: 222-233.

Oberman NG. 2008. Contemporary permafrost degradation of northern European Russia. In: Proceedings of the 9th International Conference on Permafrost, 29 June–3 July 2008,

Institute of Northern Engineering, University of Alaska, Fairbanks, Kane DL, Hinkel KM (eds). 1305–1310.

Plug LJ, Scott BM, Walls C. 2008. Tundra lake changes from 1978 to 2001 on the Tuktoyaktuk Peninsula, western Canadian Arctic. Geophysical Research Letters 35:L03502. DOI:10.1029/2007GL032303.

Rampton V M. 1988. Quaternary Geology of the Tuktoyaktuk Coastlands, Northwest Territories, Mem. Geol. Surv. Can. 423: 98.

Riordan B, Verbyla D, McGuire AD. 2006. Shrinking ponds in subarctic Alaska based on 1950–2002 remotely sensed images. Journal of Geophysical Research 111: G04002.

Romanovsky VE, Smith SL, Christiansen HH. 2010. Permafrost thermal state in the polar Northern Hemisphere during the International Polar Year 2007-2009: A synthesis, Permafrost Periglacial Processes 21.

Sannel ABK, Brown IA. 2010. High resolution remote sensing identification of thermokarst lake dynamics in a subarctic peat plateau complex: Canadian Journal of Remote Sensing. 36:S1 26-40.

Slama CC, Theurer C, Henriksen SW (Eds). 1980. Manual of Photogrammetry, American Society of Photogrammetry.

Soloviev PA. 1962. Alass relief and its origin in Central Yakutia. In: Monogoletnemerzlye porody I soputstvuscie im yavleniya na territorii Yakutskoj ASSR. Akademi Nauk SSSR, Moscow, pp. 38–53.

Sharkhuu N. 1969. Permafrost of Bulnai range's plateau. Journal of Geographic Review of Mongolia 9: 86-113.

Sharkhuu A, Sharkhuu N, Etzelmuller, Heggem ESF, Nelson FE, Shiklomanov NI, Goulden CE, Brown J. 2007. Permafrost monitoring in the Hovsgol mountain region, Mongolia. Journal of Geophysical Research 112: F02S06.

Sharkhuu N, Anarmaa Sh, Romanovsky VE, Nelson FE, Shiklomanov NI. 2008. Thermal state of permafrost in Mongolia, In: Proceeding of the Ninth International Conference on Permafrost, University of Fairbanks, Alaska, USA. 1633-1638.

Sharkhuu N. 2011. Field Guidebook to Mountain and Arid Land Permafrost in the Nalaikh and Terelj Areas near Ulaanbaatar, and in the Hovsgol and Hangai mountainous regions, Mongolia. 22-26 August 2011, Ulaanbaatar, Mongolia; 1-50.

Smith LC, Sheng Y, MacDonald GM, Hinzman LD. 2005. Disappearing Arctict lakes. Science 308: 1429.

Taube CM. 2000. Instructions for winter lake mapping. Chapter 12 in Schneider, James C. (ed.) 2000. Manual of fisheries survey methods II: with periodic updates. Michigan Department of Natural Resources, Fisheries Special Report 25, Ann Arbor.

Tumurbaatar D. 2001. Permarfrost in the Darkhad depression of Hovsgol, In: Proceeding of the International Symposium on Mountain and Arid Land Permafrost. Sharkhuu N (ed). Ulaanbaatar, Mongolia; 79-82.

Tserensodnom J. 2000. In: Catalogy of Mongolain Lakes. First Edition. Ulaanbaatar, Mongolia. Vol. 1: 1-141.

Thornthwaite CW. 1948. An approach toward a rational classification of climate: Geographical Review, Vol. 38, 55–94.

Three Methods for Computing the Volume of a Lake Clarence M. Taube Manual of Fisheries Survey Methods II: with periodic updates Suggested citation:

Wu T, Wang Q, Watanabe M, Chen J, Battogtogh D. 2009. Mapping vertical profile of discontinuous permafrost ground penetrating radar at Nalaikh depression, Mongolia. Environ Geology. 56:1577–1583.

Wu B, Lu S. 2011. Watershed Remote Sensing: Methodology and a Paradigm in Hai Baisn. Journal of Remote Sensing, 15: 201–223.

Walter KM, Zimov AS, Chanton JP, D. Verbyla FS, Chapin III. 2006. Methane bubbling from Siberian thaw lakes as a positive feedback to climate warming, Nature, 443, 71–75, doi:10.1038/nature05040.

Walter KM, Edwards ME, Grosse G, Zimov AS, Chapin III. 2007. Thermokarst lakes as a source of atmospheric CH4 during the last deglaciation, Science, 318, 633–636, doi:10.1126/science.1142924.

Yatagai A, Arakawa O, Kamiguchi K, Kawamoto H, Nodzu MI, Hamada A. 2009. A 44-year daily gridded precipitation dataset for Asia based on a dense network of rain gauges, *SOLA* 5:137-140. doi:10.2151/sola.2009-035.

Yoshikawa K, Hinzman LD. 2003. Shrinking Thermokarst Ponds and Groundwater Dynamics in Discontinuous Permafrost near Council, Alaska. Permafrost and Periglacial Processes, 14, 151-160.

Zimov SA, Voropaev YV, Semiletov IP, Davidov SP, Prosiannikov SF, Chapin III, Chapin MS, Trumbore S, Tyler S. 1997. North Siberian lakes: A methane source fueled by Pleistocene carbon, Science, 277, 800–802, doi:10.1126/science.277.5327.800.

Zhao L, Wu G, Marchenko SS, Sharkhuu N. 2010. Thermal state of permafrost and active layer in Central Asia during the International Polar Year. Permafrost and Periglacial Processes 21: 198-207.